



저작자표시-비영리-변경금지 2.0 대한민국

이용자는 아래의 조건을 따르는 경우에 한하여 자유롭게

- 이 저작물을 복제, 배포, 전송, 전시, 공연 및 방송할 수 있습니다.

다음과 같은 조건을 따라야 합니다:



저작자표시. 귀하는 원저작자를 표시하여야 합니다.



비영리. 귀하는 이 저작물을 영리 목적으로 이용할 수 없습니다.



변경금지. 귀하는 이 저작물을 개작, 변형 또는 가공할 수 없습니다.

- 귀하는, 이 저작물의 재이용이나 배포의 경우, 이 저작물에 적용된 이용허락조건을 명확하게 나타내어야 합니다.
- 저작권자로부터 별도의 허가를 받으면 이러한 조건들은 적용되지 않습니다.

저작권법에 따른 이용자의 권리는 위의 내용에 의하여 영향을 받지 않습니다.

이것은 [이용허락규약\(Legal Code\)](#)을 이해하기 쉽게 요약한 것입니다.

[Disclaimer](#)

Thesis for the Degree of Master of Engineering

Synthesis of Hollow Polystyrene Microparticles and Applications



by

Sung Hwan Park

Department of Polymer Engineering

The Graduate School

Pukyong National University

February 23, 2018

Synthesis of Hollow Polystyrene Microparticles and Applications (단분산 중공 폴리스티렌 마이크로 입자의 합성 및 응용)

Advisor : Prof. Mun Ho Kim

by
Sung Hwan Park

A thesis submitted in partial fulfillment of the requirements
for the degree of

Master of Engineering

in Department of Polymer Engineering, The Graduate School,
Pukyong National University

February 2018

Synthesis of Hollow Polystyrene Microparticles and Applications

A dissertation
by
Sung Hwan Park

Approved by:



Won Ki Lee
(Chairman) Prof, Won Ki Lee



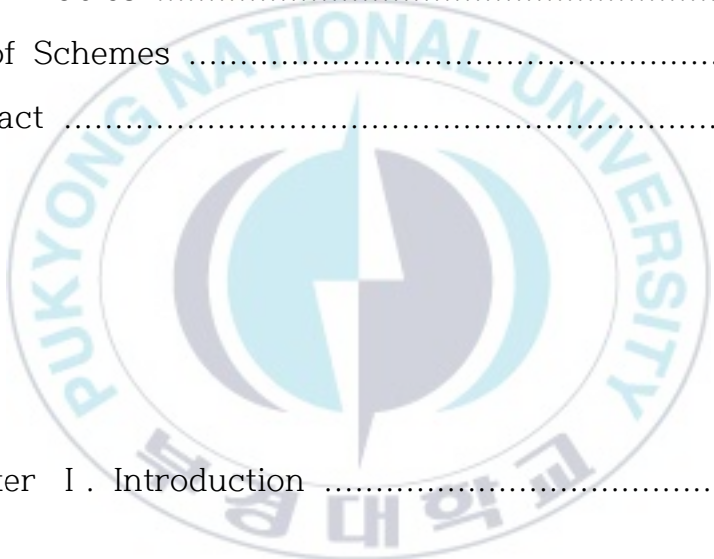
Joo Hyun Kim
(Member) Prof, Joo Hyun Kim



Mun Ho Kim
(Member) Prof, Mun Ho Kim

February 23, 2018

Contents

	Page
Contents	i
List of Figures	v
List of Tables	xi
List of Schemes	xii
Abstract	x iii
	
Chapter I. Introduction	1
I -1. Monodisperse Polymeric Microparticle	1
I -2. Suspension Polymerization	3
I -3. Emulsion Polymerization	6

I -4. Dispersion Polymerization	9
I -5. Hollow polymer particle	13
Chapter II . One-Step Synthesis of Hollow Dimpled Polystyrene Microparticles by Dispersion Polymerization	
	14
II -1. Introduction	15
II -2. Experimental section	17
II -2-1. Chemicals and Materials	17
II -2-2. Polymerization Procedures	17
II -2-3. Characterizations	18
II -3. Results and Discussion	20
II -4. Conclusions	51

Chapter III. Green Synthesis of Hollow Bimetallic Nanocrystals-Polystyrene Hybrid Microparticles and Their Catalytic Properties	53
III-1. Introduction	54
III-2. Experimental section	58
III-2-1. Chemicals and Materials	58
III-2-2. Synthesis of Polystyrene (PS) Microparticles	58
III-2-3. Fabrication of Hollow PS Microparticles	59
III-2-4. Fabrication of Ag-Embedded PS Microparticles	60
III-2-5. Fabrication of Au/Ag-Covered Hollow PS Microparticles	60
III-2-6. Fabrication of Pt/Ag-Covered Hollow PS Microparticles	61
III-2-7. Characterizations	62

III-3. Results and Discussion 63

III-4. Conclusions 86

References 87



List of Figures

Figure I -1. Schematic description of dispersion polymerization

Figure II -1. (A–C) SEM images of PS microparticles with different magnifications. (D) TEM image of PS microparticles. The v/v ratio of the ethanol to water was about 8.3, and the concentration of APS was 15 mM. The polymerization was performed at 70 °C over a period of 18 h. Scale bars represent (A) 20 μm , (B) 10 μm , (C) 2 μm , and (D) 1 μm .

Figure II -2. SEM images of products collected at different stages of the reaction: (A) t = 6 h, (B) t = 12 h, (C) t = 14 h, (D) t = 18 h, (E) t = 24 h, and (F) t = 36 h. The v/v ratio of the ethanol to water was about 8.3, and the concentration of APS was 15 mM. The polymerization was performed at 70 °C. Scale bar in each image represents 2 μm .

Figure II -3. TEM images of products collected at different stages of the reaction: (A) t = 6 h, (B) t = 12 h, (C) t = 14 h, (D) t = 18 h, (E) t = 24 h, and

(F) $t = 36$ h.

Figure II-4. Particle diameter distributions of PS microparticles collected at different stages of the reaction: (A) $t = 6$ h, (B) $t = 12$ h, (C) $t = 14$ h, (D) $t = 18$ h, (E) $t = 24$ h, and (F) $t = 36$ h.

Figure II-5. Plots of the average particle diameter and shell thickness of the PS microparticles as a function of the polymerization time.

Figure II-6. Schematic illustration of the formation and growth of hollow PS microparticles with the novel dimpled morphology.

Figure II-7. SEM images of PS microparticles obtained at different concentrations of APS while other conditions were kept the same: (A) 6 mM, (B) 12 mM, (C) 15 mM, (D) 18 mM, (E) 24 mM, and (F) 30 mM. Scale bar represents 2 μm for all main images.

Figure II-8. TEM images of PS microparticles obtained at different concentrations of APS (shown in Figure II-7): (A) 6 mM, (B) 12 mM, (C) 15 mM, (D) 18 mM, (E) 24 mM, and (F) 30 mM. Scale bar represents 2 μm for all main image

Figure II-9. Plot of the average particle diameter of the PS

microparticles as a function of the APS concentration.

Figure II -10. SEM images of PS microparticles obtained at different concentrations of PVP while other conditions were kept the same: (A) 0.25 wt % (0.005 g), (B) 0.5 wt % (0.01 g), (C) 0.75 wt % (0.015 g), and (D) 1.5 wt % (0.03 g) relative to styrene. Scale bar represents 5 μm .

Figure II -11. SEM and TEM images of PS microparticles grown in the reaction medium with different volume ratios of the ethanol to water. The v/v ratios of ethanol to water in the reaction medium were (A-B) 3.7 and (C-D) 13.0. The scale bar in the SEM image represents 2 μm .

Figure II -12. SEM image of PS microparticles shown in Figure II -2E after they had been aged in water for three months at room temperature. The scale bar represents 2 μm .

Figure II -13. SEM images of close-packed assemblies of PS microparticles with (A) spherical and (B) dimpled structures. Scale bar represents 5 μm .

Figure III -1. (A-B) SEM and TEM images of PS microparticles used as seed particles in the present study. Scale bar in Figure III -1A

represents 2 mm.

Figure III-2. (A) Photograph of PS microparticles before (left) and after (right) being aged in ethanol and water medium containing AgNO_3 and PVP at 70°C for 24 h. (B-C) SEM images of Ag nanocrystals-embedded PS microparticles after being aged in ethanol and water medium containing AgNO_3 and PVP at 70°C for 24 h. (D-F) TEM images of the Ag nanocrystals-embedded PS microparticles.

Figure III-3. High-resolution TEM image of PS microparticles shown in Figure III-2.

Figure III-4. Schematic illustration of the formation of Ag nanocrystals-embedded PS microparticles.

Figure III-5. TEM images of PS microparticles and after being aged in ethanol and water medium containing AgNO_3 and PVP at 70°C for different time periods: (A) 30 min, (B) 1 h, (C) 2 h, and (D) 5 h.

Figures III-6. (A) Photograph of Ag nanocrystals-embedded PS microparticles before (left) and after (right) being aged in ethanol and water medium containing HAuCl_4 and PVP at 70°C for 24 h. (B-C) SEM images and (D-F) TEM images of

the resulting bimetallic hybrid microparticles.

Figures III-7. EDS elemental mapping images of (A) Au/Ag bimetallic nanocrystals covered PS microparticles, and (B) Au/Ag bimetallic nanocrystals on PS microparticles. (C) Au and Ag elemental profiles along the green across the of Au/Ag bimetallic nanocrystal on PS microparticles. The scale bars in each image represents (A) 700 nm, and (B-C) 20 nm, respectively.

Figures III-8. (A) UV-vis absorption spectra of 4-NP before and after mixing with NaBH₄. (B) Time-dependent UV-vis absorption spectra and (C) plot of $\ln(A_t/A_0)$ vs time for the catalytic reduction of 4-NP by NaBH₄ in the presence of hollow Au/Ag bimetallic nanocrystals PS hybrid microparticles. (D) Recyclable catalytic ability of the hybrid microparticles for the reduction of 4-NP.

Figure III-9. (A) SEM and (B) TEM images of Ag nanocrystals-embedded PS microparticles and after being aged in ethanol and water medium containing K₂PtCl₄ and PVP at 70 °C for 24 h. (C) Time-dependent UV-vis absorption spectra

and (D) plot of $\ln(A_t/A_0)$ vs time for the catalytic reduction of 4-NP by NaBH_4 in the presence of hollow Pt/Ag bimetallic nanocrystals PS hybrid microparticles.



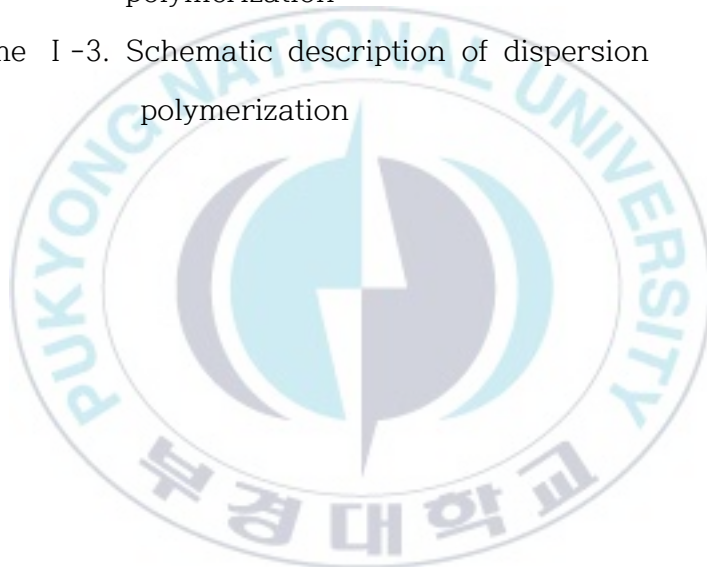
List of Tables

Table II -1. Molecular weight of PS microparticles grown with various concentrations of APS as shown in Figure II -7.



List of Schemes

- Scheme I -1. Schematic description of suspension polymerization
- Scheme I -2. Schematic description of emulsion polymerization
- Scheme I -3. Schematic description of dispersion polymerization



단분산 중공 폴리스티렌 마이크로입자의 합성 및 응용

박 성 환

부 경 대 학 교 대 학 원 고 분 자 공 학 과

요약

다양한 분야에 대한 잠재적인 유망성 때문에 중공의 형태를 가진 비구형 마이크로입자의 설계 및 합성은 매우 중요하지만, 한 번의 생산 단계만을 거치는 합성 방법의 개발은 여전히 큰 도전 과제로 남아있다. 이 연구에서 분산 중합을 기반으로 하여 새로운 template-free 방법을 성공적으로 개발하였고 이 합성방법을 통해 이방성을 가진 중공 폴리스티렌(PS) 마이크로입자를 1단계 반응으로 생산하였다. 합성에서 과황산암모늄(APS)은 매우 균일하고 안정한 중공 PS 마이크로입자의 형성 및 성장에 결정적인 역할을 담당한다. APS의 농도와 사용 된 분산안정제(폴리 비닐피롤리돈)의 농도를 변화시킴으로써 우리는 PS 입자의 평균 크기와 그 오목함의 정도를 조절할 수 있었다. 더 나아가, 용매의 흡수를 이용한 팽창 과정 및 금속 이온 치환을 사용하여, 친환경적으로 방법으로 미리 합성된 PS 마이크로입자의 표면에 다양한 종류의 금속 나노 입자를 부착 할 수 있었다. 이 금속/PS 복합체는 4-니트로페놀의 환원 반응에서 촉매로서 작용할 수 있으며 재사용이 가능하다.

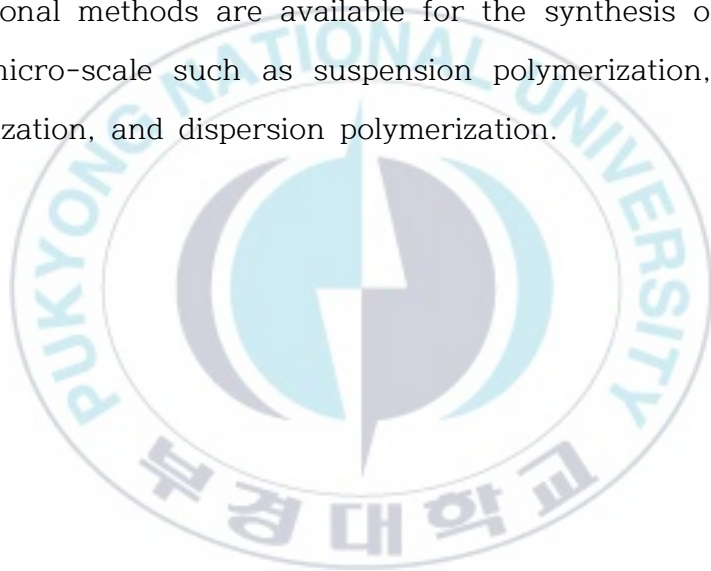
Chapter I .

Introduction

I -1. Monodisperse Polymeric Microparticle

The micro-size monodisperse polymeric spheres have received increasing attention, because of their a variety of applications, such as drug release, stimuli-responsive sensors, substrates for catalysts, and surface-functionalized particle^[1-5]. Also, polymeric microparticles are synthesized as emulsions and latex, which have already been applied as materials in the industrial fields of cosmetics, paint, composites, insulators^[6]. Many researchers have considerable attention in the synthetic process due to the increased awareness of cost, environmental issues, and technical difficulties. the mono-dispersity of microparticles have been particularly demanded since they exhibit a constant and predictable

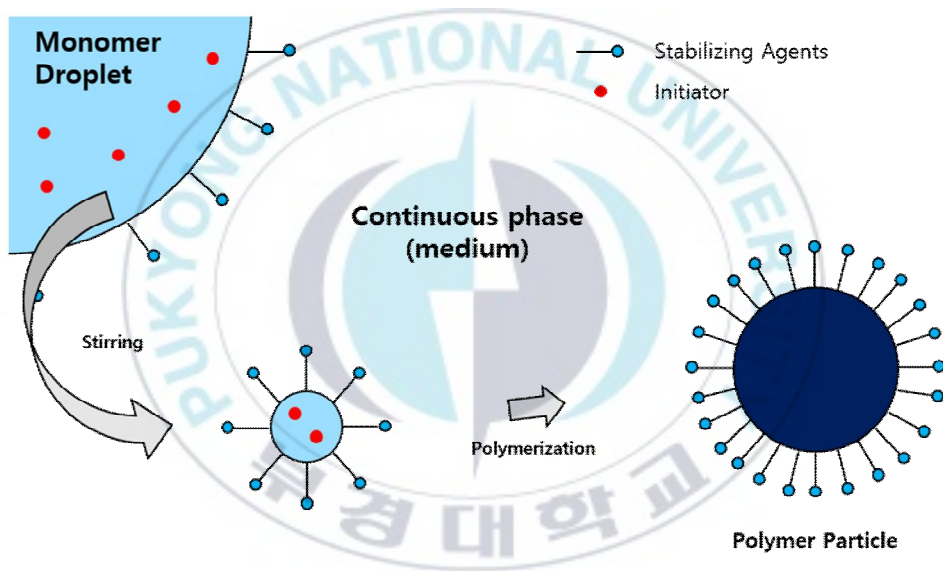
response to external fields^[7]. To date, the type of polymerization to prepare microparticles has been dominated by radical polymerization with heterogeneous systems, mainly because the parameter of polymerization was easily controlled and the amount of synthesized microparticle was bulk quantities. In general, Few conventional methods are available for the synthesis of particles under micro-scale such as suspension polymerization, emulsion polymerization, and dispersion polymerization.



I -2. Suspension Polymerization

Suspension polymerization, sometimes called bead, pearl or granular polymerization, is one of the most widely used polymerization techniques. It is consisted of a dispersing medium, stabilizing agents and monomers (Scheme I-1). Water is almost the dispersing medium. The initiator is soluble in the monomer, but both initiator and monomer are insoluble in reaction medium. The reaction medium houses mixture of reactants. As a result, the mixture constructs droplets in medium. This medium surrounding mixture easily transfers heat from droplet. So, high conversion of monomer is achieved during the reaction of polymerization^[8]. The stabilizing agent is used to prevent coalescence or agglomeration of the sticky polymer particles.

Suspension polymerization has several advantages. As above mentioned, since water is usually the continuous phase (medium), it acts as an effective heat-transfer medium which makes to easily control temperature. Resulted polymer is obtained in a bead form that is convenient and easily handled. On the contrar-



Scheme I -1. Schematic description of suspension polymerization

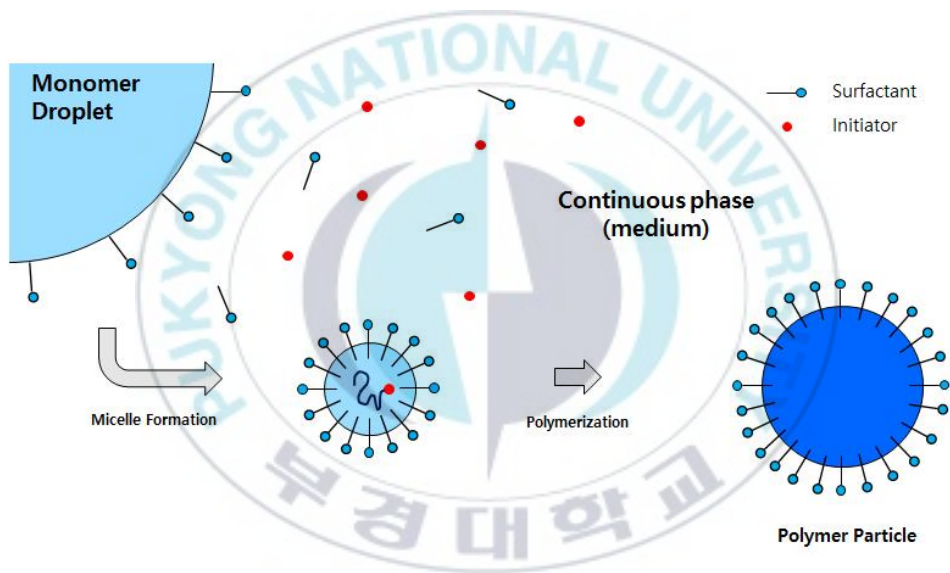
y, suspension polymerization has disadvantages. the diameter of final product depends on the diameter of droplet controlled by varying the stirring rate. In conventional suspension polymerizations, to change the stirring rate have limits. So, preparation of particles smaller than about 20 μm have become harder than other polymerization processes^[8].



I -3. Emulsion Polymerization

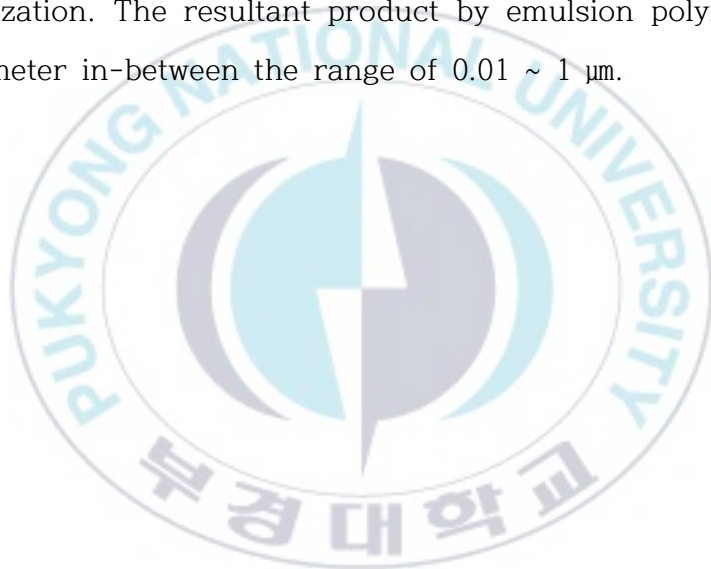
Emulsion polymerization is one of the most important methods in the production of specialty polymers^[9]. In emulsion polymerization, the most common type is an oil-in-water emulsion and polymerization system consists of a medium, monomer, surfactant, initiator (Scheme I-2). the monomer is insoluble (or scarcely soluble) in reaction medium. Unlike in suspension polymerization, the initiator is soluble in the medium and not soluble in the monomer. The surfactant forms micelles in medium. Also, the particles are hindered from coagulating with each other because each particle is surrounded by the surfactant. the concentration of surfactant is higher than critical micelle concentration (called CMC) defined as the concentration of surfactants above which micelles form. The diameter of resultant particles by emulsion polymerization has relationship with the fraction of the monomer^[10,11]. Also, a number of other factors influences the diameter of final product.

Emulsion polymerization has several advantages. it is more ra-



Scheme I -2. Schematic description of emulsion polymerization

pid than bulk or solution polymerization at the same temperature. Therefore, the average molecular weight is higher than at the same polymerization rate in bulk or solution polymerization. In addition to, the heat occurred from polymerization is easily controlled by medium like the suspension polymerization. The resultant product by emulsion polymerization has diameter in-between the range of 0.01 ~ 1 μm .



I -4. Dispersion Polymerization

Monodisperse particles with micro-size were usually difficult to obtain. Because the particles are within the size range of $0.06\ \mu\text{m} \sim 0.07\ \mu\text{m}$ by conventional emulsion polymerization and the size range of $50\ \mu\text{m} \sim 1000\ \mu\text{m}$ by conventional suspension polymerization^[6]. For this reason, Dispersion polymerization is promising method that facilitate to synthesize micro-size monodisperse particles in a single batch process. In general, the product can be yielded within $0.1\ \mu\text{m} \sim 15\ \mu\text{m}$ in diameter (Figure I -1). Also, nano-size particles with excellent monodispersity are afforded by dispersion polymerization^[12]. Dispersion polymerization is a type of precipitation polymerization, meaning the solvent selected as the reaction medium is a good solvent for the monomer, the initiator and the steric stabilizer, On the contrary, the polymer is not soluble in solvent^[13].

As the polymerization reaction proceeds, the generated nucleation is grown by incorporating oligomers in continuous phase (medium), and then the particles grow up (Scheme I -3). the ste-

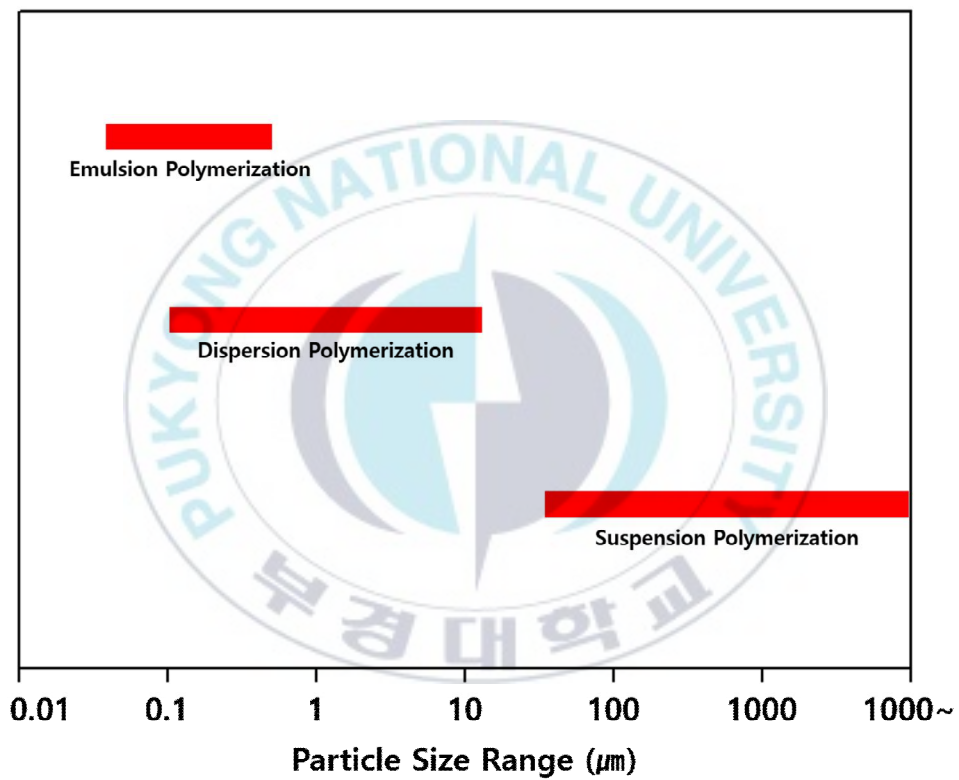
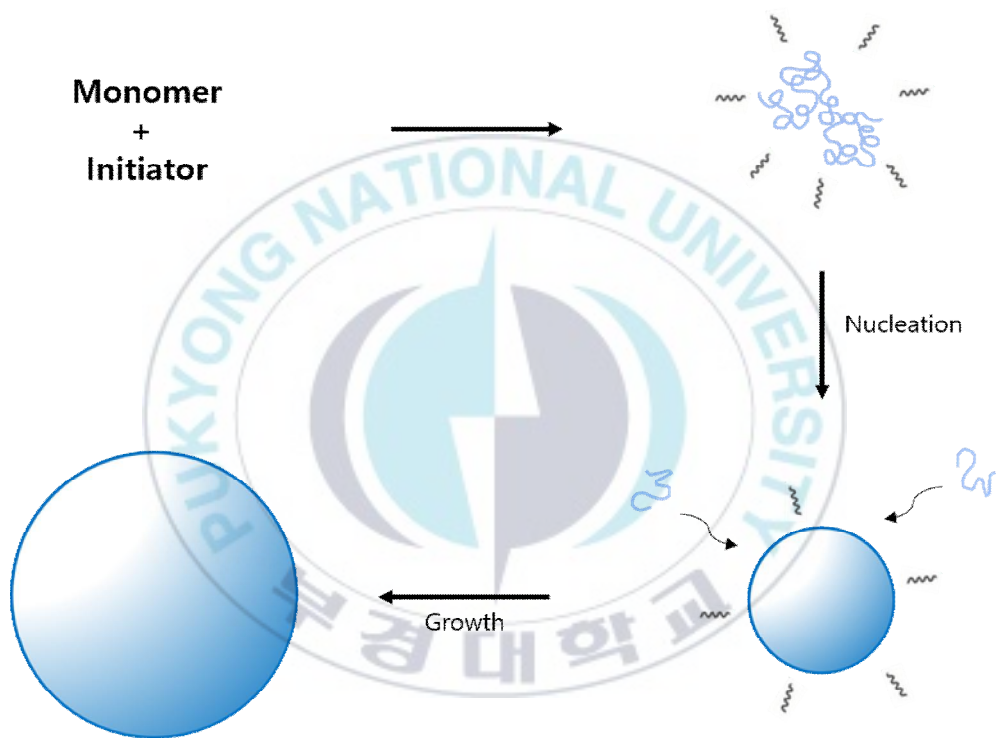


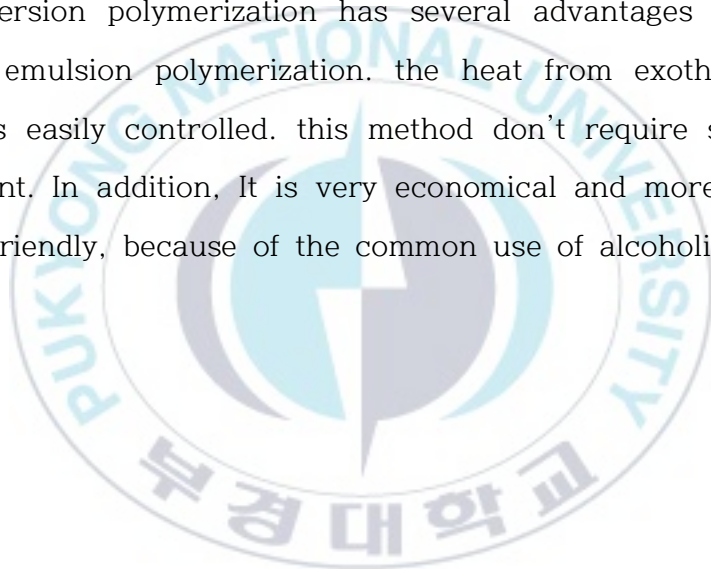
Figure I -1. Schematic description of dispersion polymerization



Scheme I -3. Schematic description of dispersion polymerization

ric stabilizers play a crucial role in the dispersion polymerization. it prevents to coagulate with each other during the reaction of polymerization. Furthermore, the steric stabilizer is related with the growth of particles directing the particle size and colloidal stability in particle formation stage^[6].

Dispersion polymerization has several advantages similar to that of emulsion polymerization. the heat from exothermic reaction is easily controlled. this method don't require specialized equipment. In addition, It is very economical and more environmental friendly, because of the common use of alcoholic aqueous solvent.



I -5. Hollow polymer particle

Hollow polymer particles play important roles in widespread use in biological and chemical applications^[14-16]. Moreover, they have potential applications applied as materials in the industrial fields of coating, papermaking, and cosmetics because of their excellent characteristics of light scattering and low density^[17]. Similarly, the monodispersity of the hollow polymer microspheres is very important to show uniform performance. The preparation of hollow microspheres has several strategies. Many researcher have recently studied for developing different routes. Hollow polymer microspheres are fabricated by removal of the core particles using chemical etching^[18], phase separation^[19], self assembly^[20], emulsion droplets^[21]. But, these different approaches for making hollow polymeric microspheres have barriers such as specialized equipment, experimental techniques. So, new approaches to easily fabricate Hollow polymer particles are required.

Chapter II .

One-Step Synthesis of Hollow Dimpled Polystyrene Microparticles by Dispersion Polymerization



Reproduced with permission from
[Langmuir, 2017, 33 (9), pp 2275-2282]
Copyright © 2017 American Chemical Society

II -1. Introduction

The synthesis and assembly of polymer nanostructures that form hollow spheres have garnered considerable attention in recent years because of their medicinal, biological, and industrial applications, including in targeted drug delivery, as catalysts, and photonic crystals, and for encapsulation of macromolecules^[22-28]. In order for the industrial applications of these nanostructures to succeed, they must meet what are becoming increasingly stringent requirements regarding particle monodispersity, porosity, shape and size. A variety of manufacturing methods, such as hard template, soft template, dynamic swelling, osmotic swelling, and polymeric micelle methods, have been developed for producing hollow polymer microparticles with well-defined nanostructures^[29-36]. However, most of these methods use a template strategy. Although the cavity size of the hollow microparticles can be easily controlled by using a sacrificial template, preparing core-shell particles requires a great deal of processing time and continuous attention and effort^[25]. In addition, in order to form

hollow structures, the cores need to be removed by using dissolving or drying techniques, which require specialized equipment and harsh processing environments. Seeded polymerization is more direct and does not require template removal, but the method is not a one-step synthesis involving forming seed particles in advance, followed by the polymerization^[37-39].



II -2. Experimental section

II -2-1. Chemicals and Materials

Styrene (product no. S4972, 2.5 L), ammonium persulfate (APS), polyvinylpyrrolidone (PVP; $M_w \approx 55$ kDa), and ethanol (product no. 459844-1 L) were received from Aldrich. All chemicals were used without further purification. The deionized (DI) water (product AH365-4, 4 L) used in the reaction was a product of SK Chemicals (Republic of Korea).

II -2-2. Polymerization Procedures

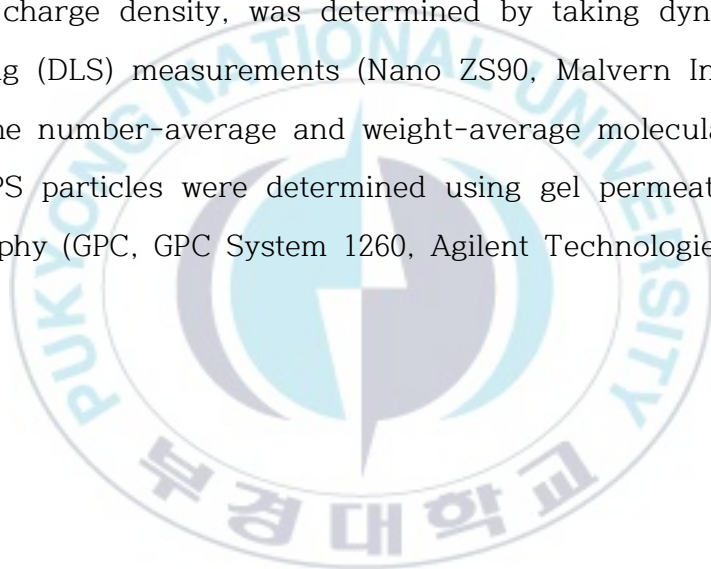
The dispersion polymerization of styrene was conducted in a mixture of ethanol and water with APS as an initiator. The polymerization was carried out in a 50 mL vial with magnetic stirring. Preweighed PVP and initiator were first added into the

vial. The mass of PVP in a typical polymerization was 0.01 g (0.5 wt % relative to styrene). The concentration of APS was varied from 6 to 30 mM. Then, 25 mL of ethanol and 3 mL of deionized water were poured into the vial. The mixture was stirred well with a magnetic bar for 10 min at room temperature. Finally, a volume of 2.2 mL of styrene monomer was added and the polymerization temperature was fixed at 70 °C in an oil bath. The reaction was carried out with sufficient stirring. After completion of the polymerization, any further reaction was quenched by placing the vial in ice water for 30 min. The product was collected after centrifuging the vial at 13,000 rpm and rinsed off repeatedly with deionized water to remove the residual styrene and PVP.

II -2-3. Characterizations

Scanning electron microscopy (SEM) images were recorded using a field-emission scanning electron microscope (Sirion, FEI) operated at an accelerating voltage of 10 kV. Transmission electron microscopy (TEM) images were obtained using a Philips

Tecnai F30 microscope operated at 200 kV. The SEM (or TEM) sample was prepared by placing a drop of the final product (suspended in DI water) on a silicon wafer (or carbon-coated copper grid), and then drying the sample in a fume hood. The zeta potential of the PS colloidal particles, which reflects their surface charge density, was determined by taking dynamic light scattering (DLS) measurements (Nano ZS90, Malvern Instruments Ltd.). The number-average and weight-average molecular weights of the PS particles were determined using gel permeation chromatography (GPC, GPC System 1260, Agilent Technologies).



II -3. Results and Discussion

Dispersion polymerization is an attractive and promising alternative to other polymerization methods and affords micrometer-size monodisperse particles in a single batch process^[45,46]. The dispersion polymerization of a monomer is carried out in the presence of a suitable polymeric steric stabilizer that is soluble in the reaction medium, and also involves the use of an initiator. A key feature of dispersion polymerization is that the solvent selected as the reaction medium should be a good solvent for both the monomer and the steric stabilizer, but a nonsolvent for the polymer being formed. Thus, dispersion polymerization is defined as a type of precipitation polymerization^[47]. In this study, polyvinylpyrrolidone (PVP) was used as the steric stabilizer, and ammonium persulfate (APS) was used as the initiator. Though APS is a well-known initiator commonly used in emulsion polymerization, it has been rarely used in dispersion polymerization. Since APS cannot be dissolved in pure ethanol, a mixture of ethanol and water was used as the reaction medium.

The prepared PS microparticles were observed by using SEM and TEM. In a typical synthesis, PVP with an average molecular weight of 55 kDa and a mass content of 0.5 wt % relative to styrene was used. The v/v ratio of ethanol to water in the reaction medium was about 8.3. The concentration of APS was 15 mM, and the polymerization was carried out for 18 h. Highly monodisperse particles with an average size of 2.07 (± 0.03) μm were obtained (Figure II-1A,B). No particles aggregated and the size distribution was quite narrow. Figure II-1C shows magnified SEM images of the microparticles, whose morphologies were observed to be not plain spheres, but instead concave spheres. To further demonstrate the concave feature of the PS microparticles, the same particles were investigated using TEM. A dimple was clearly observed on the surface of each particle (Figure II-1D). The most striking feature observed in the TEM image was the strong contrast between the dark edge and the bright center, which indicated that the particles were not solid, but were hollow. The average diameter of the cavity and thickness of the PS shell were determined from the image in Figure II-1D to be approximately 1.64 and 0.43 μm , respectively. These results reve-

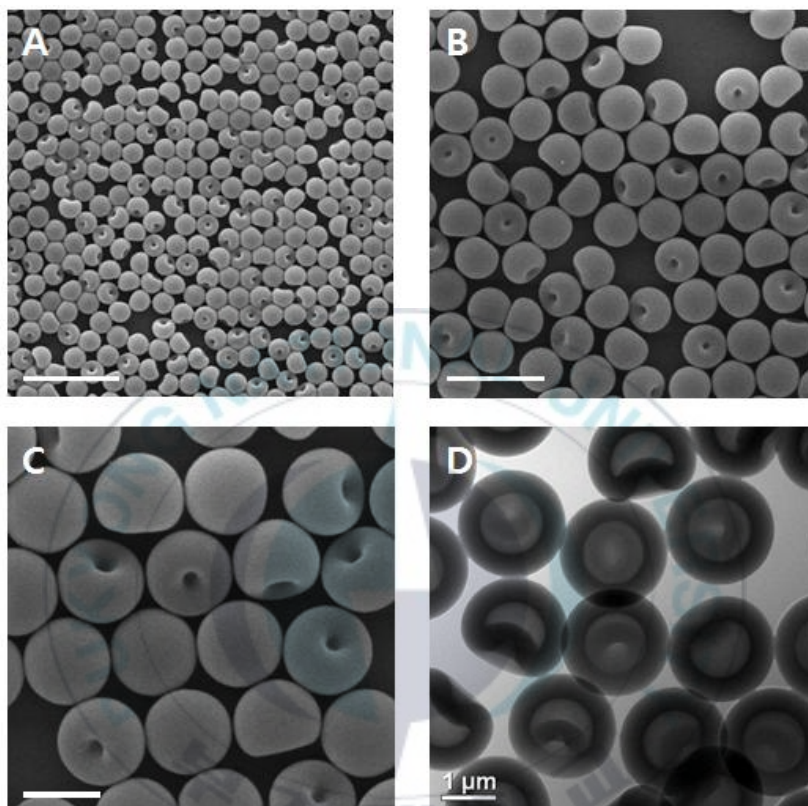


Figure II -1. (A–C) SEM images of PS microparticles with different magnifications. (D) TEM image of PS microparticles. The v/v ratio of the ethanol to water was about 8.3, and the concentration of APS was 15 mM. The polymerization was performed at 70 °C over a period of 18 h. Scale bars represent (A) 20 μm , (B) 10 μm , (C) 2 μm , and (D) 1 μm .

ealed that uniform hollow and dimpled PS microparticles could be successfully synthesized via dispersion polymerization in a single step, and without using any templates. We are not the first group to observe the formation of particles with anomalous structures in the heterophase polymerization process. The formation of particles with similar morphology to the PS particles shown in Figure II-1 in the course of surfactant-free emulsion polymerization has been reported for many decades^[48-53]. However, to the best of our knowledge, a synthesis of hollow PS microparticles with the described novel morphology using a simple one-step dispersion polymerization method without a template has not been reported previously.

The growth of the dimpled hollow microparticles was examined by monitoring the evolution of their shapes. This monitoring was accomplished by conducting a series of reactions under identical conditions except for stopping the reactions at various time points. Figure II-2 shows SEM images of typically synthesized PS microparticles after the various reaction times. These images indicated that at each reaction time, the produced PS particles showed a very narrow size distribution. Their sizes and shapes,

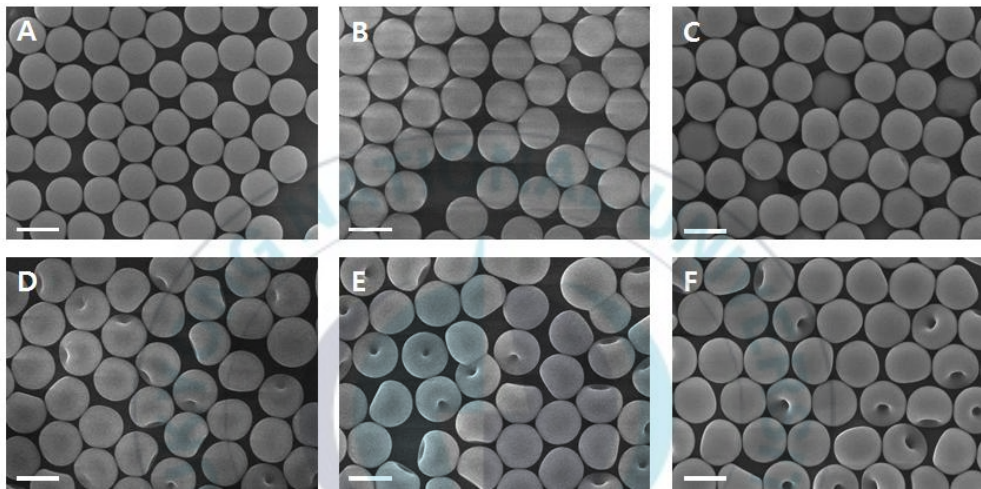


Figure II -2. SEM images of products collected at different stages of the reaction: (A) $t = 6$ h, (B) $t = 12$ h, (C) $t = 14$ h, (D) $t = 18$ h, (E) $t = 24$ h, and (F) $t = 36$ h. The v/v ratio of the ethanol to water was about 8.3, and the concentration of APS was 15 mM. The polymerization was performed at 70 °C. Scale bar in each image represents 2 μm .

however, did change with reaction time. During the first 6 h of the reaction, the products were mainly spherical particles with an average diameter of $1.71 (\pm 0.02) \mu\text{m}$ and without any dimples on their surfaces. After a reaction of 12 h, no notable change was observed in the shape of the particles, as shown in Figure II-2B. However, the average diameter of the PS microparticles increased to $1.92 (\pm 0.02) \mu\text{m}$. After a reaction time of 14 h, the average diameter of the particles was observed to increase to $1.97 (\pm 0.02) \mu\text{m}$, and a small concavity was observed on the surface for many of the otherwise spherical particles (Figure II-2C). As shown in Figure II-2D, when the reaction was prolonged to 18 h, the concave feature became more obvious and was observed on the surface of nearly every particle. The PS particles became severely deformed and anisotropic after a reaction time of 24 h, as shown in Figure II-2E, and their average diameter increased to $2.19 (\pm 0.04) \mu\text{m}$. Note that the PS microparticles did not grow any more after 24 h: as shown in the SEM image of Figure II-2F, the particles obtained after a reaction time of 36 h displayed an average diameter of $2.17 (\pm 0.03) \mu\text{m}$. The surface dimple on each particle did, however, become on average a bit larger.

Figure II-3 shows TEM images taken from the same samples depicted in Figure II-2. Figure II-3A shows a TEM image of the particles obtained after a 6 h reaction time. This image revealed that each of the particles produced in the early stage of the polymerization had a solid structure. When the reaction was prolonged to 12 h, the corresponding TEM image, shown in Figure II-3B, clearly indicated that the particles each contained a small interior cavity. As the reaction time was increased to 14 h, the particles were observed to become slightly asymmetric and the interior cavity of each particle became larger (Figure II-3C). As the reaction time was further increased, the extent of the concavity was observed in the TEM images to increase, as it was observed in the SEM images. After the reaction time of 18 h, the particles were observed in the corresponding TEM image (Figure II-3D) to have a nearly uniform shell thickness of $0.43 (\pm 0.01) \mu\text{m}$, nearly 41% of the value of the average particle radius. The dimple on the particle surface and the resulting concave structure that were observed in the corresponding SEM image were also observed in this TEM image. Prolonging the reaction times

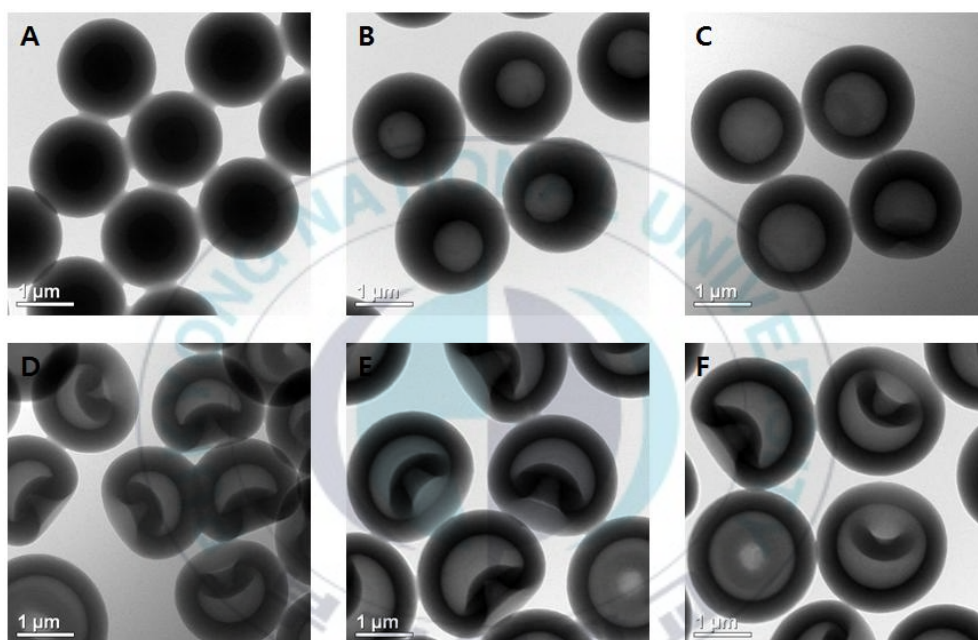


Figure II-3. TEM images of products collected at different stages of the reaction: (A) $t = 6$ h, (B) $t = 12$ h, (C) $t = 14$ h, (D) $t = 18$ h, (E) $t = 24$ h, and (F) $t = 36$ h.

to 24 h (Figure II-3E) resulted in a continued increase in the size of the cavity, and the shell thickness correspondingly decreased to 0.39 μm at this stage of reaction; the volume of the cavity, however, was reduced due to the growth of the dimple. After the reaction time was increased to 36 h, the shell thickness, as shown in the TEM image of Figure II-3F, slightly decreased to 0.36 μm and the volume of the cavity became quite small with the further growth of the dimple. Figure II-4 shows size distributions of the PS particles shown in Figures II-2 and II-3. A plot of the average diameter of the PS microparticles and the average shell thickness as a function of the reaction time is also shown in Figure II-5. The average diameter of the particles was observed to increase linearly with reaction time for the first approximate 18–24 h of reaction and then to gradually plateau with the further increase in reaction time.

The structural transformation observed during the polymerization may be explained by the following proposed mechanism. It is first helpful to understand the particle growth as having been divided into two phases: the first one involving the transformation of the solid particle into the hollow particle over the course of t-

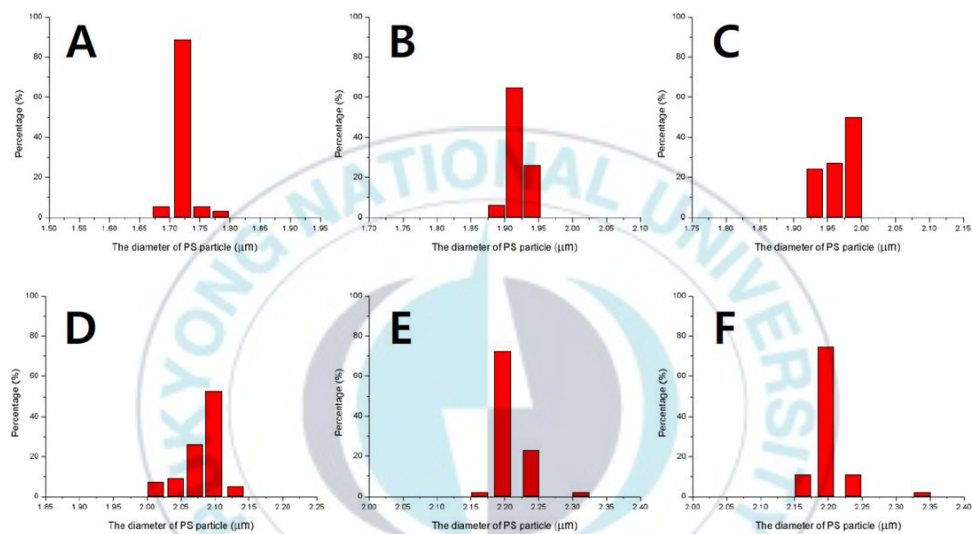


Figure II-4. Particle diameter distributions of PS microparticles collected at different stages of the reaction: (A) $t = 6$ h, (B) $t = 12$ h, (C) $t = 14$ h, (D) $t = 18$ h, (E) $t = 24$ h, and (F) $t = 36$ h.

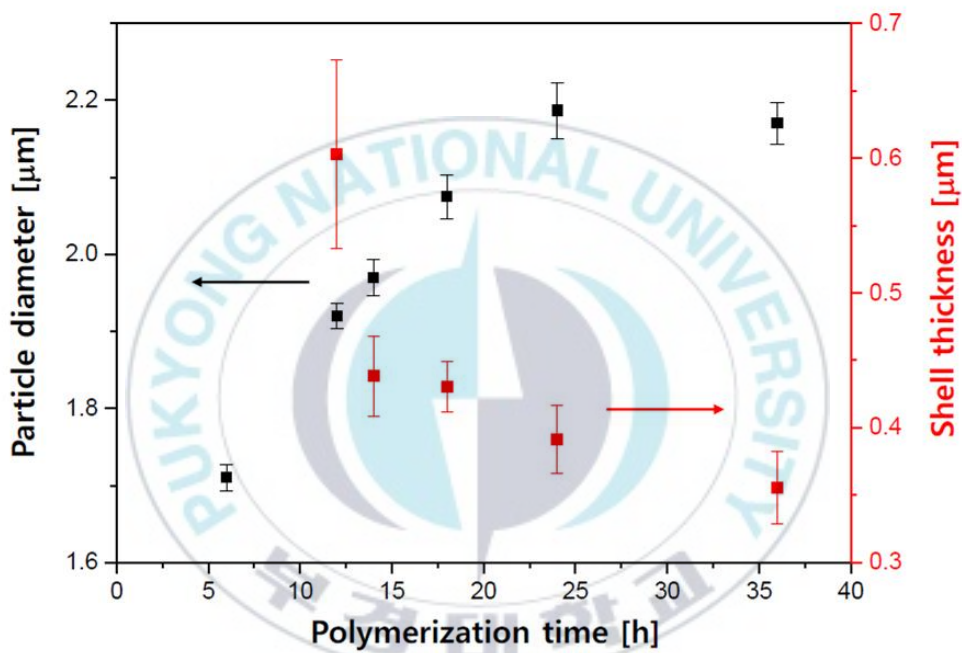


Figure II-5. Plots of the average particle diameter and shell thickness of the PS microparticles as a function of the polymerization time.

he first 14 h of the reaction; and the second one marked by the hollow structure undergoing a buckling process. At the start of the reaction, the monomer, stabilizer and initiator were dissolved in the mixture of ethanol and DI water to form a homogeneous solution. According to the proposed mechanism, upon heating this resulting mixture, the initiator decomposed and the free radicals reacted with monomers to form oligomer radicals; then, when the oligomers grew to a critical chain length, they became immiscible in the reaction mixture and adsorbed stabilizer to form a stable particle; and once particles were formed, they absorbed monomers from the continuous phase, and they became swollen with these monomers^[54]. From this stage on, according to the proposed mechanism, polymerization preferentially took place on the particle surface because the surface adsorbed and anchored the aqueous radicals formed from the APS molecules dissolved in the water^[25]. Accordingly, the particle surface in this mechanism served as the subsequent polymerization locus for the monomers infusing from the center of the particle. Gradually, the polymer chains migrated from the center of the particle to the surface together with the monomers, resulting in the formation

of the cavity as shown in Figure II-3B. The difference between the average solid volume of the PS particles resulting from a reaction time of 12 h (Figure II-3B) and that from a reaction time of 6 h (Figure II-3A) was calculated from the radii (r) of the particle and cavity to be about $0.76 \mu\text{m}^3$ by using the expression:

$$\left(\frac{4}{3}\pi((r_{12h})^3 - (r_{6h})^3 - (r_{cavity})^3)\right)$$

This increase in the solid volume despite the formation of the cavity indicated that polymerization kept on taking place on the particle surface.

According to the proposed mechanism, since further polymerization caused a rapid consumption of monomers inside the swollen particles, the hollow microspheres experienced deswelling, giving rise to mechanical stress at the polymer shells. Therefore, the shells buckled at the relatively thin sites as shown in Figure II-3C. The shell deformation allowed the structure to adopt the buckled shape with a single dimple. In the present study, no particles with more than one dimple were observed, which suggested that the deswelling process was slow. In elastic theory, the pressure-induced collapse of a thin spherical shell is a well-known problem, and the minimum pressure required for buckling, called

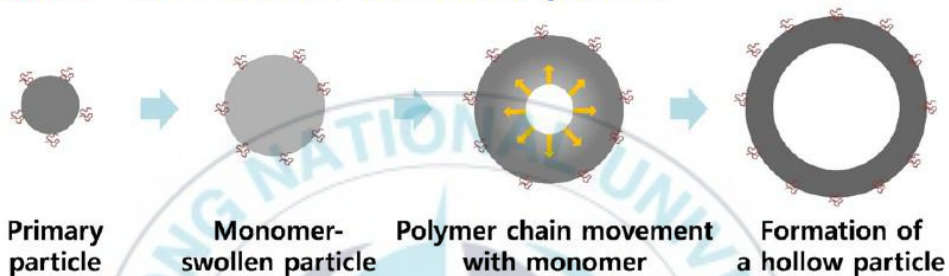
the critical pressure (ρ_c), can be given by:

$$\rho_c \propto Y_0 \left(\frac{h}{R_0} \right)^2 \quad (1)$$

where Y_0 is the 3D Young's modulus and h and R_0 are the initial shell thickness and the initial spherical shell radius, respectively^[55]. The relationship indicates that a large thin shell can be buckled easily, which explains why the buckling of the PS particles occurred when the small solid particles grew into hollow large particles with thin shell thickness (see particles in Figure II-3D resulting from the 18 h reaction). Finally, particles with highly anisotropic structures were produced after a reaction time of 24 h, when the monomers were apparently depleted. Figure II-6 shows a schematic representation of the mechanism for the formation and growth of the hollow dimpled PS microparticles, based on the results shown in Figures II-2 and II-3.

In the present study, both the size and shape of the microparticles could be adjusted by tuning the experimental parameters of the polymerization. For example, the concentration of the APS initiator was found to have a significant influence on the both the size and morphology of the particle. Dispersion poly-

Phase 1 : Formation of the hollow particle



Phase 2 : Buckling process

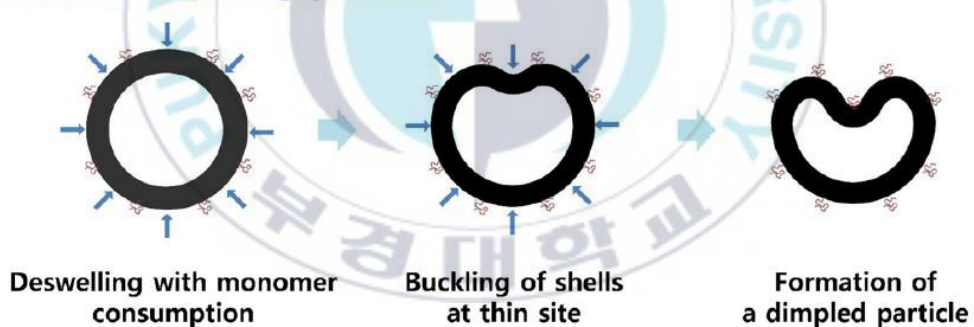


Figure II -6. Schematic illustration of the formation and growth of hollow PS microparticles with the novel dimpled morphology.

rizations were carried out with various concentrations of APS, from 6 to 30 mM. Figure II-7 shows the SEM images of the samples polymerized for 18 h with these different APS concentrations. The results indicated that PS microparticles with diameter ranging from 1.49 to 3.05 μm can be obtained by changing the concentration of APS. Although monodisperse PS particles were obtained with concentrations of APS below 24 mM, secondary particles were generated when using 30 mM APS. Thus, initially increasing the concentration of the initiator led to uniformly larger particles, while increasing the concentration further to a high level produced a more complex result. We expect that at higher initiator concentrations, the proportion of produced oligomers would also increase. Such an increase would result in a faster growth of polymer microspheres, and increased aggregation of precipitated oligomers would produce larger particles^[56,57]. For very high APS concentrations, excessively high reaction rates would interfere with the addition of newly formed oligomers on the existing particles, but favor self-nucleation, leading to the formation of the secondary particles, as we observed for an APS concentration of 30 mM (Figure II-7F).

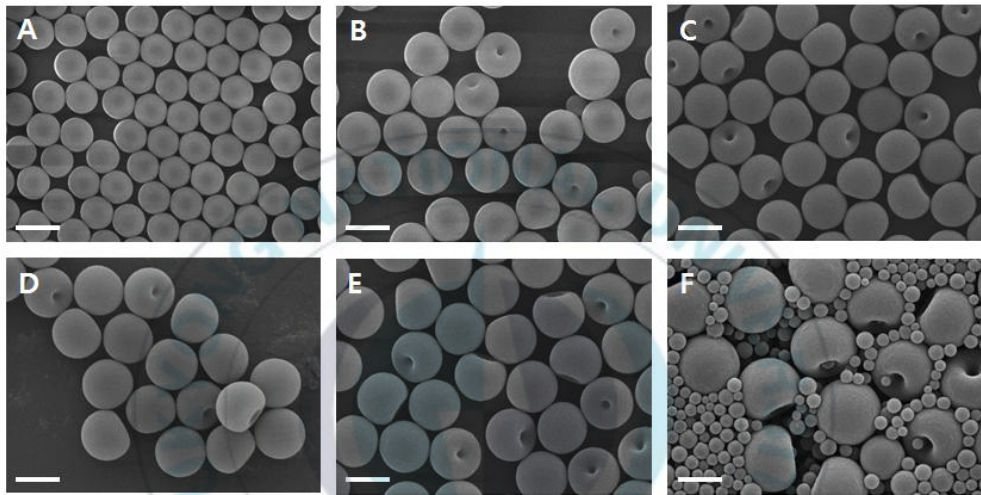


Figure II -7. SEM images of PS microparticles obtained at different concentrations of APS while other conditions were kept the same: (A) 6 mM, (B) 12 mM, (C) 15 mM, (D) 18 mM, (E) 24 mM, and (F) 30 mM. Scale bar represents 2 μm for all main images.

Figure II-8 show TEM images of the PS particles grown with the various concentrations of APS. These particles were observed in the TEM images to be spherical and hollow. They were also observed to have a dimpled structure, except for the particles obtained with 6 mM APS (Figure II- 7A). As described above, of all APS concentrations tested, 6 mM APS yielded the smallest particle. Based on the TEM image, the particles had relatively thick shells, which would result from the high molecular weight of the polymer. For a fixed amount of monomer, the molecular weight of the polymer is inversely proportional to the concentration of initiator in the radical polymerization. Molecular weights of the PS particles grown with different concentrations of APS were measured by gel permeation chromatography (GPC) and summarized in Table II -1. The results confirmed that the sample shown in Figure II- 7A had the highest molecular weight value. The lack of dimples in the particles obtained with 6 mM APS is consistent with eq 1, which predicts the need for relatively high pressures to lead to the buckling of small particles with somewhat thick shells. A plot of the average observed diameter of the microparticles a function of the tested APS concentration is sho-

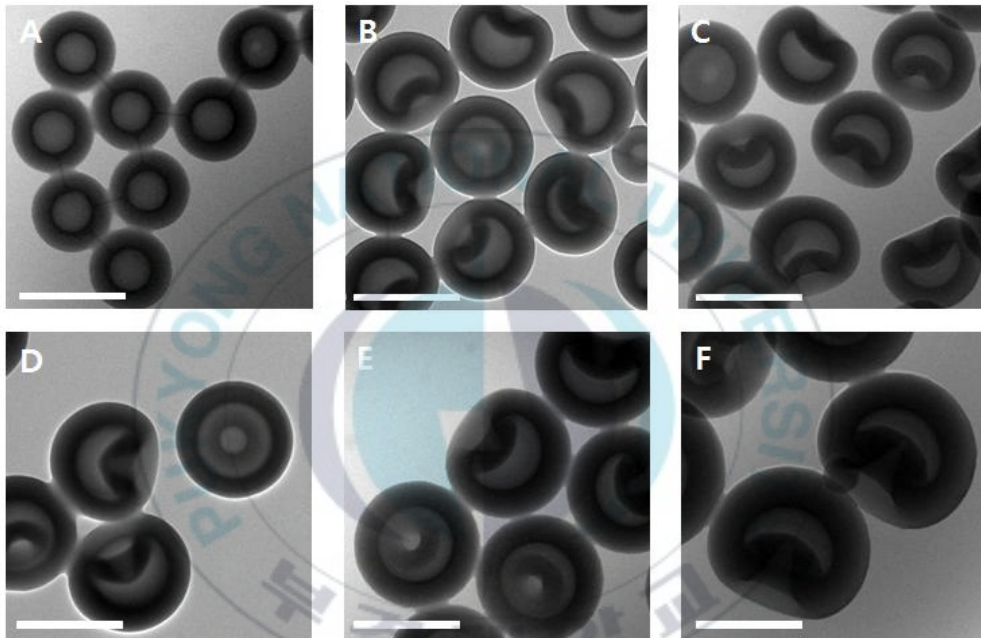


Figure II-8. TEM images of PS microparticles obtained at different concentrations of APS (shown in Figure II-7): (A) 6 mM, (B) 12 mM, (C) 15 mM, (D) 18 mM, (E) 24 mM, and (F) 30 mM. Scale bar represents 2 μm for all main image

APS concentration [mM]	M_n	M_w	Polydispersity (=M_w/M_n)
6	24499	115619	4.72
12	12302	73459	5.97
15	9700	59370	6.12
18	8657	55889	6.46
24	7586	49636	6.54

Table II-1. Molecular weight of PS microparticles grown with various concentrations of APS as shown in Figure II-7.

wn in Figure II-9. This plot revealed a nearly linear relationship between the microparticle size and concentration of APS from 1 to 30 mM.

The influence of the concentration of PVP concentration was also tested. Figure II-10 shows SEM images of the PS particles synthesized with various PVP concentrations. When the concentration of PVP was 0.25 wt %, some particles aggregated as shown in Figure II-10A, indicating that the PS particles were not sufficiently stabilized by such a low PVP concentration. Unaggregated monodisperse PS particles were obtained when the concentration of PVP is 0.5 wt % (Figure II-10B). For PVP concentrations of 0.75 and 1.50 wt %, in addition to the main particles, secondary small particles were also observed, and thus the monodispersity became worse, as shown in Figures II-10C and II-10D. Overall, as the concentration of PVP was increased from 0.25 to 1.50 wt %, the average diameter of the dimpled (main) particles decreased from $2.35 (\pm 0.04) \mu\text{m}$ to $1.76 (\pm 0.02) \mu\text{m}$. In dispersion polymerization, the ultimate size of the particles depends on the number of nuclei formed in the early stages of polymerization. An increase in the number of nuclei, while keepi-

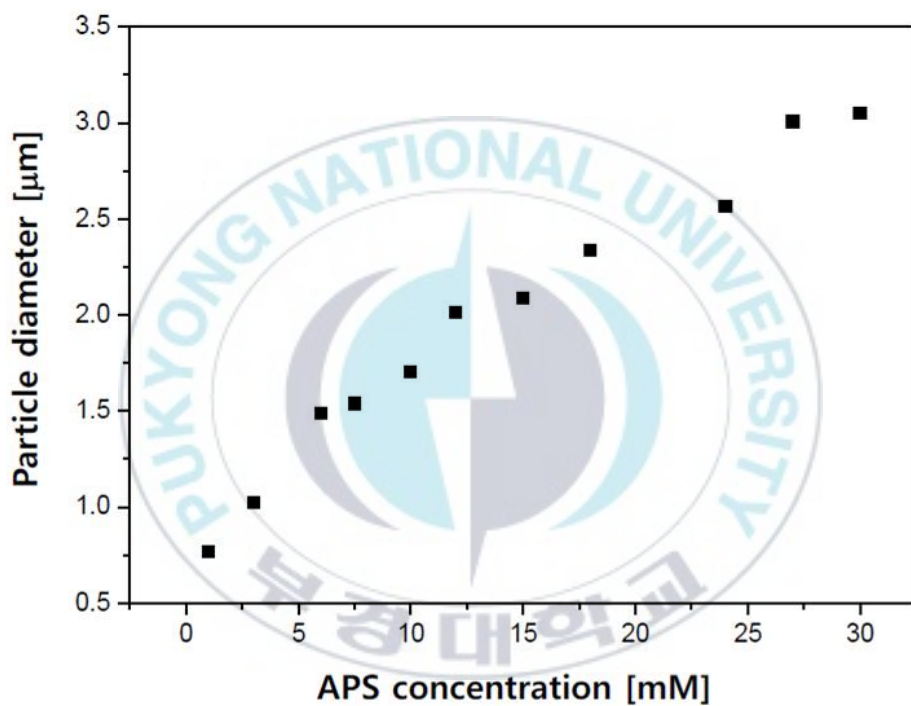


Figure II -9. Plot of the average particle diameter of the PS microparticles as a function of the APS concentration.

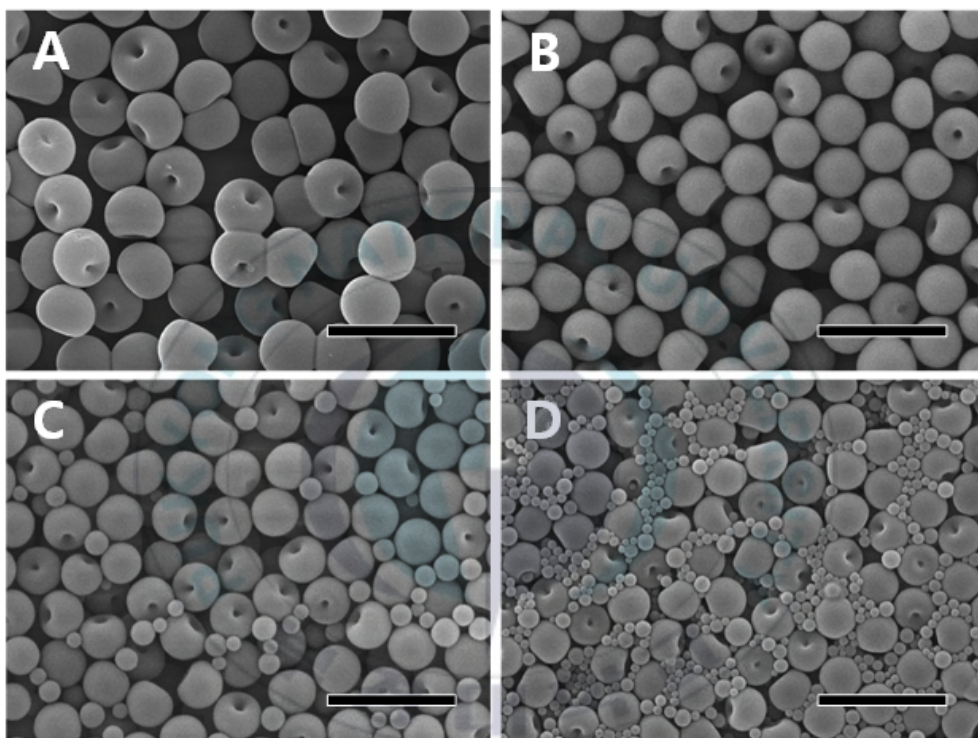


Figure II -10. SEM images of PS microparticles obtained at different concentrations of PVP while other conditions were kept the same: (A) 0.25 wt % (0.005 g), (B) 0.5 wt % (0.01 g), (C) 0.75 wt % (0.015 g), and (D) 1.5 wt % (0.03 g) relative to styrene. Scale bar represents 5 μm .

ng the concentration of monomer the same, would be expected to result in the formation of smaller polymer particles. In a typical dispersion polymerization, the nucleation starts partially on the stabilizer backbone via a hydrogen abstraction^[56,57]. Therefore, the stabilizer polymer provides supplementary nucleation sites, which can explain why in our experiments the particle size depended inversely on the concentration of stabilizer and why secondary particles were generated for high concentrations of stabilizer.

It is worth noting that a volume ratio of ethanol to water in the reaction medium also played a crucial role in the formation of the dimpled hollow microparticles. In the above experiments, the v/v ratio of ethanol to water in the reaction medium was fixed as 8.3. Doubling the volume of water, which decreased the ratio of ethanol to water to 3.7, yielded a sample containing small spheres, as shown in Figure II-11A. Figure II-11B shows a TEM image of the sample, indicating that the spheres displayed a hollow structure. According to the mechanism proposed, the formation of hollow structures resulted from the use of the aqueous radical formed from APS, which is soluble in water. When the v-

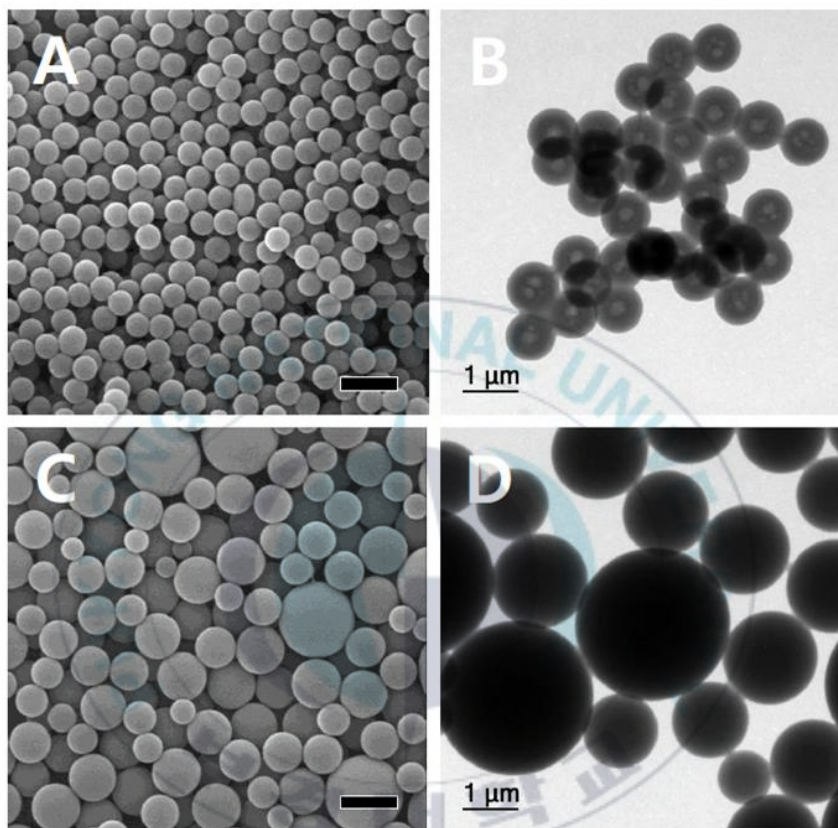


Figure II-11. SEM and TEM images of PS microparticles grown in the reaction medium with different volume ratios of the ethanol to water. The v/v ratios of ethanol to water in the reaction medium were (A-B) 3.7 and (C-D) 13.0. The scale bar in the SEM image represents 2 μm .

olome fraction of water in the solvent system increased, the number of nuclei formed in the early stages of polymerization also increased due to enhanced mobility of the aqueous radical, which resulted in particle size reduction of final particles. By contrast, increasing the ratio to 13.0 by decreasing the volume of water to 1/2 yielded polydisperse solid spheres as shown in Figure II-11C and II-11D, which indicates that the reaction did not proceed homogeneously due to lack of water.

In contrast to the solid spheres, the dimpled hollow micro-particles were likely thermodynamically unstable, considering a relatively high surface energy and the buckled structures. As mentioned above, the buckling process occurred slowly during the growth of the particles, indicating that they formed under kinetically controlled reaction conditions. Thermodynamically unstable particles tend to aggregate and sediment because formation of the resulting colloid tends to reduce surface energy. To evaluate their stability, we aged the PS particles in water at room temperature for three months. Interestingly, the particles obtained in the present study kept the concave surface shapes and no aggregation of the particles was observed, as shown in

Figure II-12. That is, despite the high surface energy, these dimpled hollow particles exhibited excellent stability, which can be attributed mainly to the PVP stabilizer. Note that in the present study, however, only 0.5 wt % of PVP relative to styrene was used because secondary particles formed when using higher concentration of PVP over 0.75 wt % as shown in Figure II-10. Considering that dispersion polymerizations usually use 2–10 wt % stabilizer relative to styrene monomer to keep their shape and prevent aggregation, the current PS particles were able to be stabilized by a quite low concentration of the PVP stabilizer.

The excellent stability of the PS particles can be explained by the dual roles of the APS, which has ionic characteristics^[57]. When APS decomposes, the persulfate generates radicals according to eq 2 and initiates a polymerization reaction.



During the polymerization, the sulfate group becomes part of the polymer and can act as an electrostatic costabilizer. By using DLS, the zeta potential of the PS particles was measured and found to have a value of -51.4 mV. This result reflected the negative surface charge of the synthesized PS particles, which r-

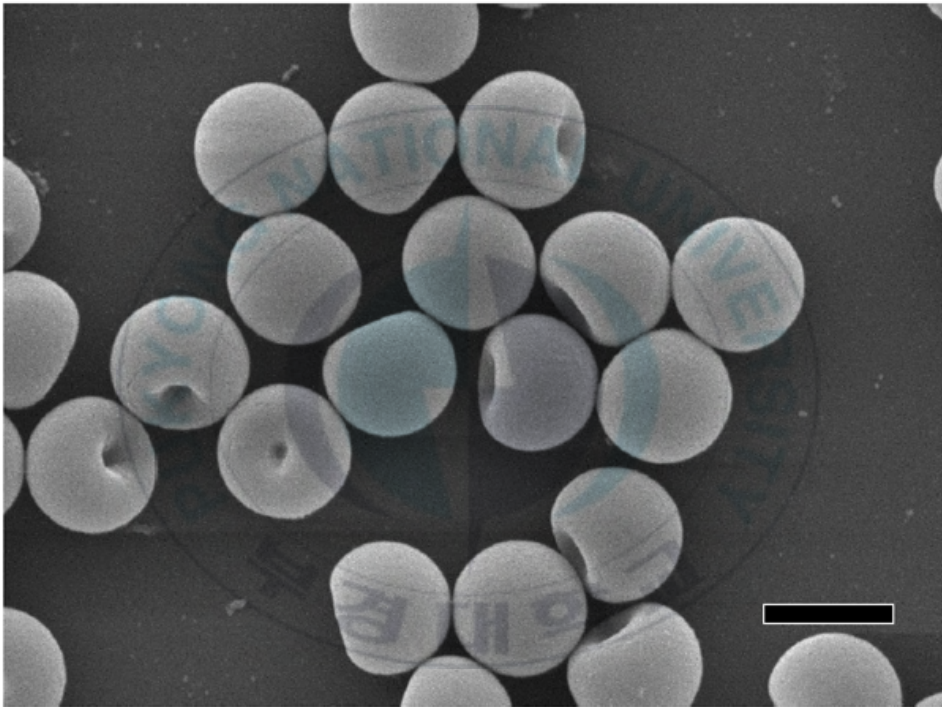


Figure II -12. SEM image of PS microparticles shown in Figure II -2E after they had been aged in water for three months at room temperature. The scale bar represents 2 μm .

esulted from the attachment of the sulfate groups ($[\text{OSO}_3]^-$) to the surfaces. The aggregation of PS particles was thus apparently hindered by electrostatic stabilization. Because they made use of a combination of two mechanisms, namely electrostatic and steric stabilization, the PS particles produced in the present study were highly stable.

One important measure of the effectiveness of a method for synthesizing colloids is whether the method can produce colloidal particles of uniform size. Uniform particle assemblies and their derivatives have been widely applied for various applications. Because of the use of APS as an initiator with ionic characteristics, aggregation of the particles was prevented despite the low concentration of PVP. Using a low rather than a high concentration of this stabilizer suppresses was shown above to be necessary for avoiding the formation of secondary particles, and thus led to the formation of highly monodisperse particles. Generally, uniform spherical particles tend to assemble into a close-packed lattice (either hexagonal closepacked (HCP) or face-centered cubic (FCC) structure). In order to confirm the uniformity of the PS microparticles obtained in the present study,

colloidal crystals of these particles were produced by applying the convective assembly method^[58]. The spherical particles obtained after 12 h of polymerization were able to assemble into a highly ordered close-packed lattice, specifically a hexagonal array, as shown in Figure II-13. The dimpled particles obtained after 24 h of polymerization were also found to form this type of lattice. Note that because of the concave shape, the surface of the crystal of the dimpled particles showed some voids larger than any of the voids in the crystal of the undimpled particles. Taken together, the above results confirmed the uniformity of the particles produced in the present study.

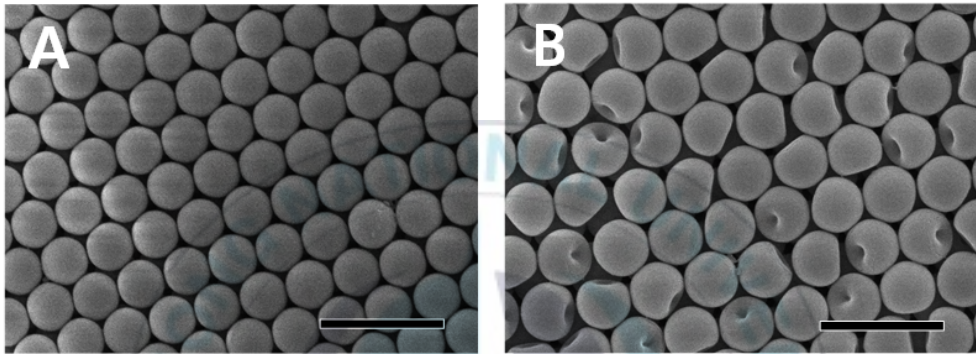


Figure II-13. SEM images of close-packed assemblies of PS microparticles with (A) spherical and (B) dimpled structures. Scale bar represents 5 μ m.

II -4. Conclusions

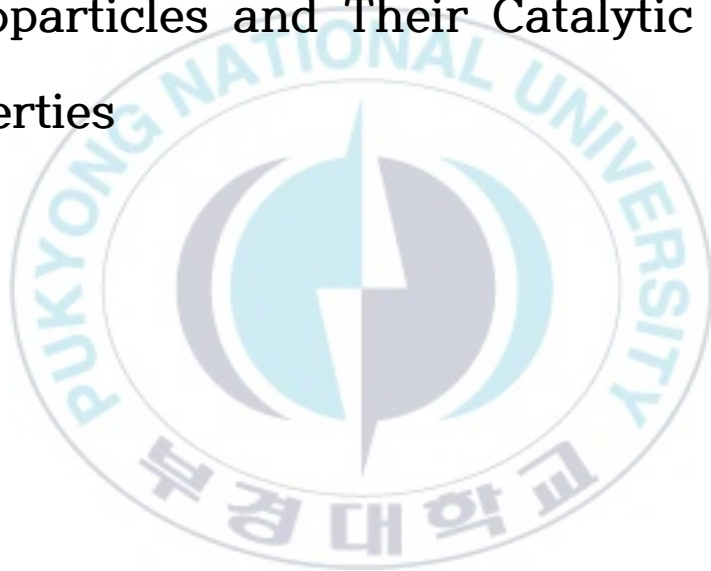
Hollow dimpled polystyrene (PS) microparticles were synthesized using a one-step dispersion polymerization method that adopted the heterophase polymerization system, without using any template. During the reaction, the solid spherical particles transformed into hollow particles, which then underwent a buckling process to form the hollow dimpled PS microparticles. The average diameter of the microparticles and the degree of concavity of the dimpled surface can be tuned to some extent by varying the reaction conditions. The experimental results revealed that ammonium persulfate (APS) played a critical role in the formation and growth of the PS microparticles. The hollow dimpled PS particles produced in this study were quite uniform, enough so that they could assemble into a close packed lattice, and they showed excellent stability with regards to their dispersity and shape. This study not only advanced our understanding of the roles played by APS in dispersion polymerization, but also provides unprecedented opportunities to synthesize polymer particles with

controlled nanostructures.



Chapter III.

Green Synthesis of Hollow Bimetallic Nanocrystals-Polystyrene Hybrid Microparticles and Their Catalytic Properties



III-1. Introduction

Metal nanocrystals have garnered considerable attention because of their numerous applications in electronic, chemical, biological, and medical fields due to their distinctive properties, when compared to their bulk counterparts^[59-62]. Among them, noble metal nanocrystals have been used as effective catalysts with high reactivity and excellent selectivity^[63-68]. These catalytic properties of metal nanocrystals can be tailored for a specific application by controlling their size, shape, and composition. However, one major problem that needs to be addressed in the usage of metal nanocrystals as catalysts is their strong tendency of aggregation to minimize their surface area^[69-72]. In order to solve this problem, metal nanocrystals have been deposited on the surface of supports to form colloidal composite particles. Various support including polymers, silica, carbon structures, titania, and dendrimers have been developed to immobilize metal nanocrystals, which allows the nanocrystals to retained high stability and activity, and enable easy and effective separation from the

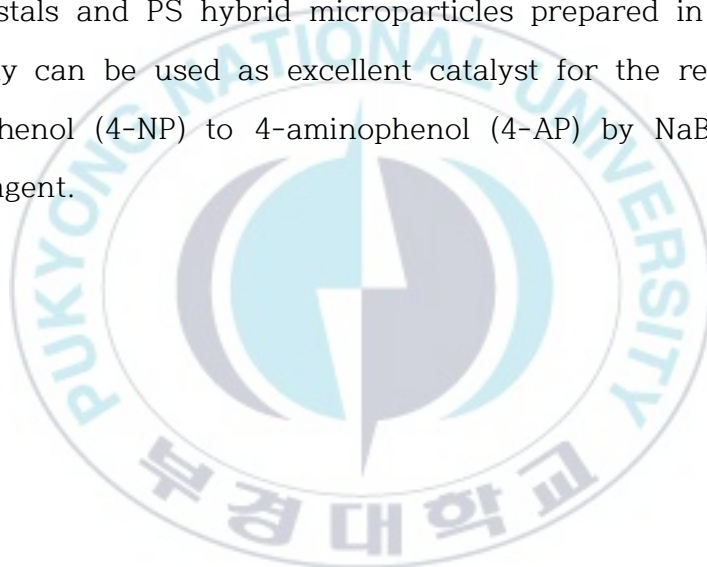
reaction mixture for reuse^[71-77].

Generally, the immobilization of metal nanocrystals on the surface of solid supports has been demonstrated by forming metal nanocrystals, followed by blending the nanocrystals and support materials^[78-79]. To define and direct metal nanocrystals onto the solid supports, surface pretreatments were usually applied to enhance the interaction between metal nanocrystals and the surface of solid supports^[70,72]. These *ex situ* processes and surface modification require a great deal of processing time and continuous attention and effort, which complicated the synthetic procedures^[80,81]. However, a facile synthesis of metal nanocrystal and support hybrid nanostructures via an *in situ* method has not yet been developed and is hence of particular interest.

In this paper, we report a new and facile method for producing metal nanocrystals covered polystyrene hybrid microparticles. This method used a simple procedure involving the mixing metal ions with as-prepared Ag nanocrystals-embedded seed, which were dispersed in an ethanol-water mixture. This new synthetic route has several distinctive features over previously reported procedures. First, the new synthetic method was found to be a

facile protocol based on *in situ* production of metal nanocrystals from metal precursor on the polymer particles, without involving forming metal nanocrystals in advance. In addition, the surface pretreatment of the polymer particles were not indispensable at all. Secondly, the synthetic procedures were environmentally acceptable green chemistry method. Although most of the studies on the reduction of metal atoms from the metal precursor have been relied on toxic reducing agent such as NaBH₄, hydrazine, DMF and organic solvent, a non-toxic reducing agent and environmentally benign solvent media were used in the present study. Thirdly, galvanic replacement reactions were successfully applied to produce bimetallic nanocrystal deposited polystyrene microparticles. It is well known that bimetallic nanocrystals have showed distinctive catalytic properties, which are clearly different from those of monometallic nanoparticles^[82-85]. Finally, the polystyrene microparticles have a hollow structure. Due to the presence of air cavity, the microparticle produced has a low bulk density and high surface-to-volume ratio, which is suited for the supporting materials for catalyst. We monitored the morphological and structural changes during the formation of the hybrid

microparticles, and a plausible mechanism was proposed, based on the observations and experimental results. The features mentioned above motivated us to explore the catalytic activity of the hollow bimetallic (Au/Ag and Pt/Ag) nanocrystals and PS hybrid microparticles. It was demonstrated that the hollow bimetallic nanocrystals and PS hybrid microparticles prepared in the present study can be used as excellent catalyst for the reduction of 4-nitrophenol (4-NP) to 4-aminophenol (4-AP) by NaBH_4 as reducing agent.



III-2. Experimental section

III-2-1. Chemicals and Materials

Styrene (product No. S4972, 2.5 L), ammonium persulfate (APS), polyvinylpyrrolidone (PVP; $M_w \approx 55$ kDa), ethanol (product No. 459844-1L), silver nitrate (product No. 209139, 100 g), and gold(III) chloride trihydrate (product No. 520918, 1g) were received from Aldrich (USA). All chemicals were used without further purification. The deionized (DI) water (product AH365-4, 4 L) used in the reaction was a product of SK Chemicals (Republic of Korea).

III-2-2. Synthesis of Polystyrene (PS) Microparticles

Spherical PS microparticles were synthesized following our previously reported one-pot synthetic method. 0.01 g of Pre-weighed

PVP and APS (15 mM) were first added into the 50mL vial. Then, 25 mL of ethanol and 3mL of deionized water were poured into the vial. After the mixture was stirred with a magnetic bar for 10 min at room temperature, the styrene monomer (2.2 mL) was added. The vial was brought in an oil bath at 70 °C. The reaction was carried out for 6 h, and then quenched by placing the vial in ice water for 30 min. The product was collected after centrifuging the vial at 6,000 rpm and rinsed off repeatedly with deionized water.

III-2-3. Fabrication of Hollow PS Microparticles

The synthesized PS microspheres (0.02 g) were dispersed in 1mL DI water. The PS dispersion was poured in to 20 mL vial. Then, 5 mL of ethanol was injected in vial. The vial was put into oil bath at 70 °C and stirred at 400 rpm with a magnetic bar. After the reaction for 24 hr, the vial was placed in ice water for 30 min and rinsed off repeatedly with deionized water mentioned above.

III-2-4. Fabrication of Ag-Embedded PS Microparticles

Pre-weighed PVP (0.003g) and 1mL of aqueous solution containing AgNO_3 (177mM) were added into 20 mL vial. The PS aqueous dispersion (0.03 g/1 mL) and 5 mL of ethanol were poured in to 20 mL vial. The vial was put into oil bath at 70 °C and stirred at 400 rpm with a magnetic bar. After the reaction for 24 hr, the vial was placed in ice water for 30 min and rinsed off repeatedly with deionized water mentioned above.

III-2-5. Fabrication of Au/Ag-Covered Hollow PS Microoparticles

0.3 mL of aqueous solution of Ag embedded in PS microparticle and 5 mL of Ethanol were poured into 20 mL vial. Then, 0.2 mL of PVP aqueous solution (0.05 g/10 mL) and 0.5 mL of aqueous HAuCl_4 solution (1mM) were injected in vial. The vial was put into oil bath at 70 °C and stirred at 400 rpm with a magnetic bar. After the reaction for 24 hr, the vial was placed in ice water for

30 min and rinsed off repeatedly with deionized water mentioned above.

III-2-6. Fabrication of Pt/Ag-Covered Hollow PS

Microparticles

0.3 mL of aqueous solution of Ag embedded in PS microparticle and 5 mL of Ethanol were poured into 20 mL vial. Then, 0.2 mL of PVP aqueous solution (0.05 g/10 mL) and 0.5 mL of aqueous K_2PtCl_4 (1mM) solution were injected in vial. The vial was put into oil bath at 70 °C and stirred at 400 rpm with a magnetic bar. After the reaction for 24 hr, the vial was placed in ice water for 30 min and rinsed off repeatedly with deionized water mentioned above.

III-2-7. Characterizations

Scanning electron microscopy (SEM) images were recorded using a field-emission scanning electron microscope (JSM-6700F, JEOL) operated at an accelerating voltage of 15 kV. The SEM sample was prepared by placing a drop of the final product (suspended in DI water) on a silicon wafer. The transmission electron microscopy (TEM) sample was prepared by placing a drop of the final product (suspended in DI water) on a carbon-coated copper grid, and the sample was dried in a fume hood. The sample was washed with DI water to remove the remaining PVP, and then dried and stored in a vacuum. TEM analysis was performed using a Philips Tecnai F30 microscope operated at 300 kV. The zeta potential of the fabricated micro-particles, which reflects their surface charge density, was determined by taking dynamic light scattering (DLS) measurements (ELS-8000, OTSUKA Electronics).

III-3. Results and Discussion

Micron-sized monodisperse PS particles which were used as supporting materials in the present study were produced by dispersion polymerization of styrene in ethanol and water medium^[86]. Compared to other polymerization methods, dispersion polymerization is an attractive and promising alternative, producing micron-size monodisperse particles in a single batch process^[87-88]. The dispersion polymerization of a monomer is carried out in the presence of a suitable polymeric steric stabilizer that is soluble in the reaction medium. Dispersion polymerization is defined as a type of precipitation polymerization because the solvent selected as the reaction medium is a good solvent for both the monomer and the steric stabilizer, but a non-solvent for the polymer being formed^[89]. In this study, polyvinylpyrrolidone (PVP) and ammonium persulfate (APS) were used as the steric stabilizer and the initiator in order to produce PS microparticles by the dispersion polymerization. Figure III-1A presents a SEM image of prepared PS microparticles, revealing that highly monodisperse

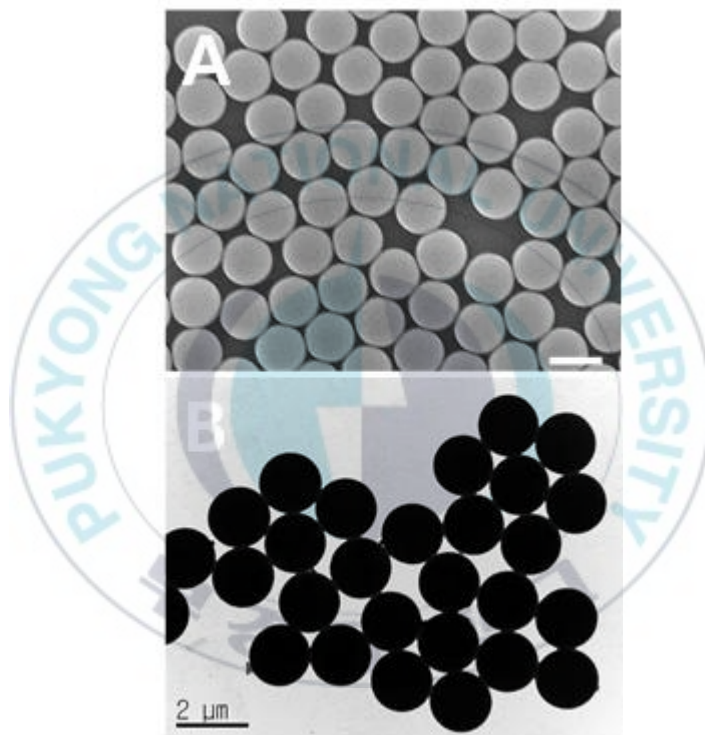


Figure III-1. (A-B) SEM and TEM images of PS microparticles used as seed particles in the present study. Scale bar in Figure III-1A represents 2 μm .

particles with an average size of 1.84 (\pm 0.02) μ m were obtained. No particles aggregated and the size distribution was quite narrow. Figure III-1B shows the TEM image of the PS microparticle, which revealed that the PS microparticles had a solid structure.

The inclusion of metal nanocrystals embedded in the hollow polymer microparticles may be expected to impart additional beneficial properties and extend its uses to applications such as antimicrobial agents, separation materials, and catalysts^[90-92]. In order to fabricate PS/metal hybrid microparticles, AgNO₃ as a metal precursor was introduced into the ethanol and water medium. The PS particles used in this study showed the excellent colloidal stability in the ethanol and water medium, which was chiefly ascribed to the repulsion force arisen from the sulfate groups that were anchored onto the surface of PS particles^[86]. However, the addition of salt ions such as AgNO₃ could hinder the electrostatic stabilization, and thus the PS particles were aggregated in addition of AgNO₃. Therefore, PVP which had been used as the steric stabilizer in the synthesis of the polymer microparticles was also further added together with addition of AgNO₃. When PS seed

microparticles were aged in ethanol and water medium containing AgNO_3 and PVP at $70\text{ }^\circ\text{C}$, the resulting colloidal solution displayed a yellowish color, as shown in Figure III-2A, which indicated that a significant change occurred. Figures III-2B exhibited the SEM images of the resulting PS microparticle, but no notable change was observed in the size and shape of particles when compared to the original PS microparticles, and a magnified SEM image (Figure III-2C) of these particles appeared to show its having smooth surfaces, indicating that few Ag nanoparticles were located on these surface. However, TEM image revealed that the small Ag nanoparticles $> 10\text{ nm}$ in size formed inside the PS microparticles, as shown in Figures III-2D-III-2F. These nanoparticle appeared crystalline (see Figure III-3), with a lattice distance $\sim 0.24\text{ nm}$, which is the same as that of (111) plane of Ag nanocrystals^[93]. These results confirmed that Ag nanocrystals were formed and embedded onto PS microparticles successfully.

The formation of Ag nanocrystals-embedded PS microparticles can be explained by the following proposed mechanism. The sulfate groups anchored onto the surfaces of PS microparticles attracted Ag^+ ions via the electrostatic attraction. The adsorbed Ag^+

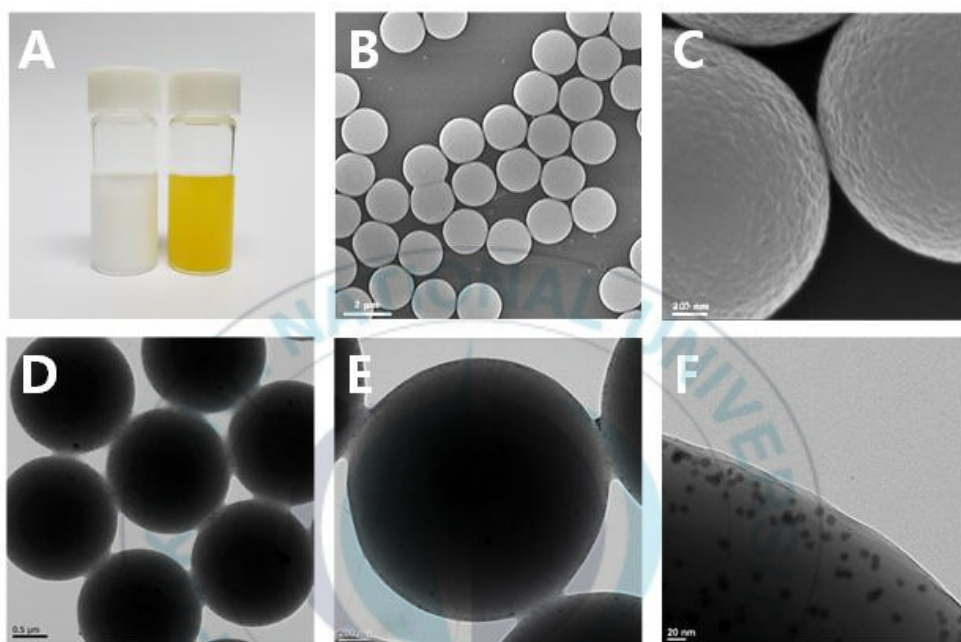


Figure III-2. (A) Photograph of PS microparticles before (left) and after (right) being aged in ethanol and water medium containing AgNO_3 and PVP at $70\text{ }^\circ\text{C}$ for 24 h. (B-C) SEM images of Ag nanocrystals-embedded PS microparticles after being aged in ethanol and water medium containing AgNO_3 and PVP at $70\text{ }^\circ\text{C}$ for 24 h. (D-F) TEM images of the Ag nanocrystals-embedded PS microparticles.

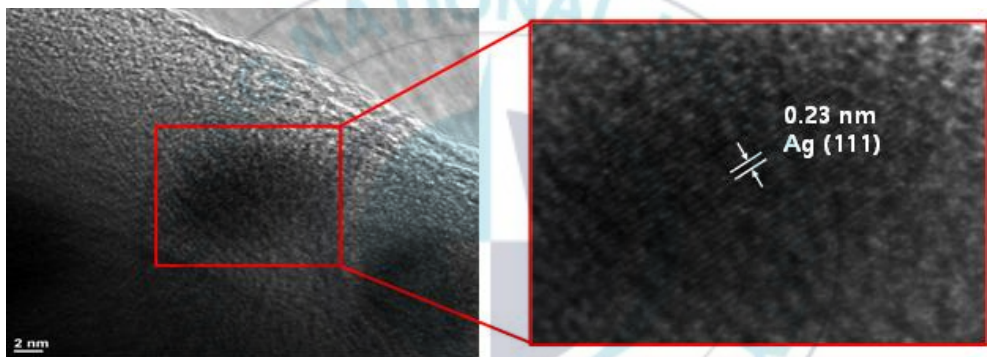


Figure III-3. High-resolution TEM image of PS microparticles shown in Figure III-2.

ions were reduced by ethanol, and then the Ag atoms came together to form large aggregates (nanocrystals). Below the glass transition temperature of the polymer, the formed nanocrystals would be initially immobilized on the surface of the PS microparticles. However, when the seed particles were dispersed in ethanol and water medium at 70 °C, the PS microparticles could be swollen by continuous phase, which is much more pronounced in dispersion polymerization compared with aqueous emulsion polymerization^[94-96]. Accordingly, the polymer chains were relaxed, which allowed the polymer chains a high degree of mobility, resulting in wetting of the nanocrystal surfaces by the polymers because of the difference in surface energy between the nanocrystals and polymers^[97-99]. Therefore, Ag nanocrystals could be embedded into the PS microparticles.

Figure III-4 shows a schematic representation of the mechanism for the formation of Ag nanocrystals-embedded PS microparticles. It is quite interesting that the formed Ag nanocrystals-embedded PS microparticles kept the original solid structure because previous studies reported that the structural transformation from solid to hollow was observed during the agi-

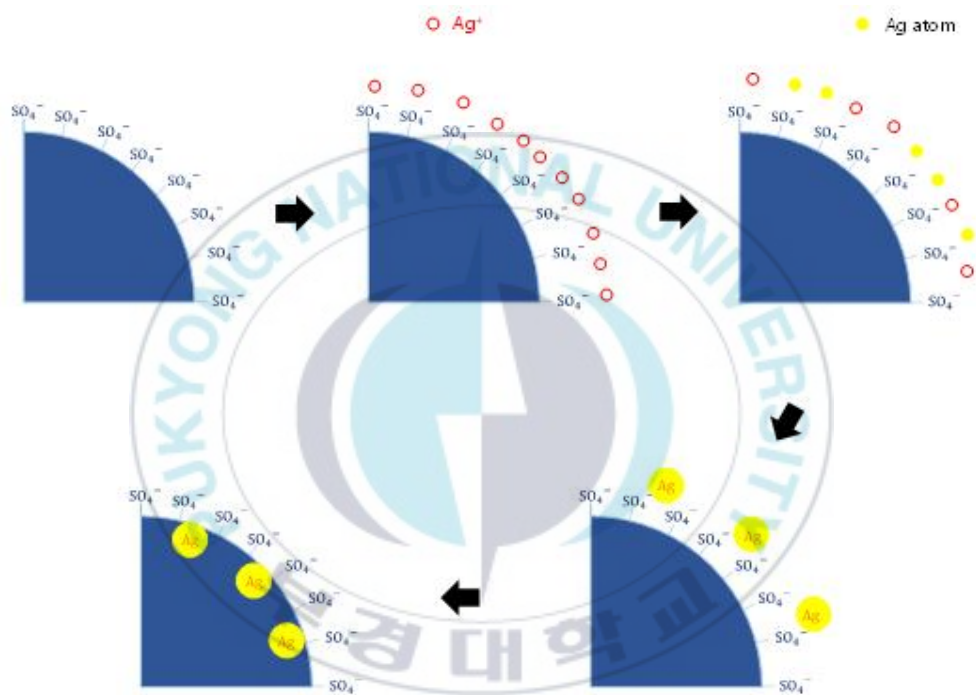


Figure III-4. Schematic illustration of the formation of Ag nano-crystals-embedded PS microparticles.

ng process. The structure transformation would be directly related to the uptake of continuous phase by the particles, which is much more pronounced in dispersion polymerization. In the present study, at the early stage of aging process, the particles revealed the hollow structures as shown in Figure III-5A, which is a TEM image of the PS microparticle aged for 30 min in the ethanol and water medium containing AgNO_3 . In the figure, large interior cavities were clearly shown. When the aging time was extended to 5 h, however, the average diameter of the PS microparticles kept decreasing and the interior cavity also became smaller (Figures III-5B-III-5D). It was expected that the ethanol and water absorbed in the early stage of aging process migrated to outside the particles. We believe that this phenomenon is related to the osmotic pressure acting from the PS microparticle inside out. As mentioned above, Ag^+ ions were adsorbed onto the particles' surface by the negatively charged sulfate groups through electrostatic attraction, and thus the surface would be covered uniformly with Ag^+ ions. Accordingly, the water molecules in the inside of the particles can be drawn to the outside the solutions with high concentration of Ag^+ ions because of the

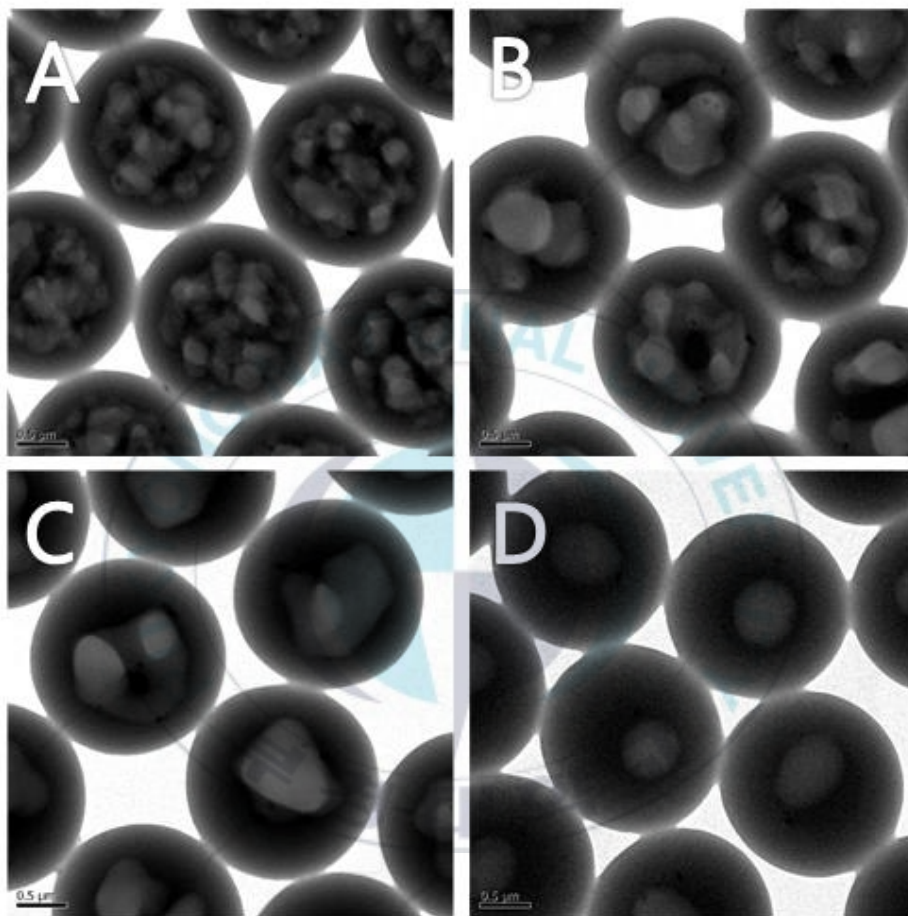
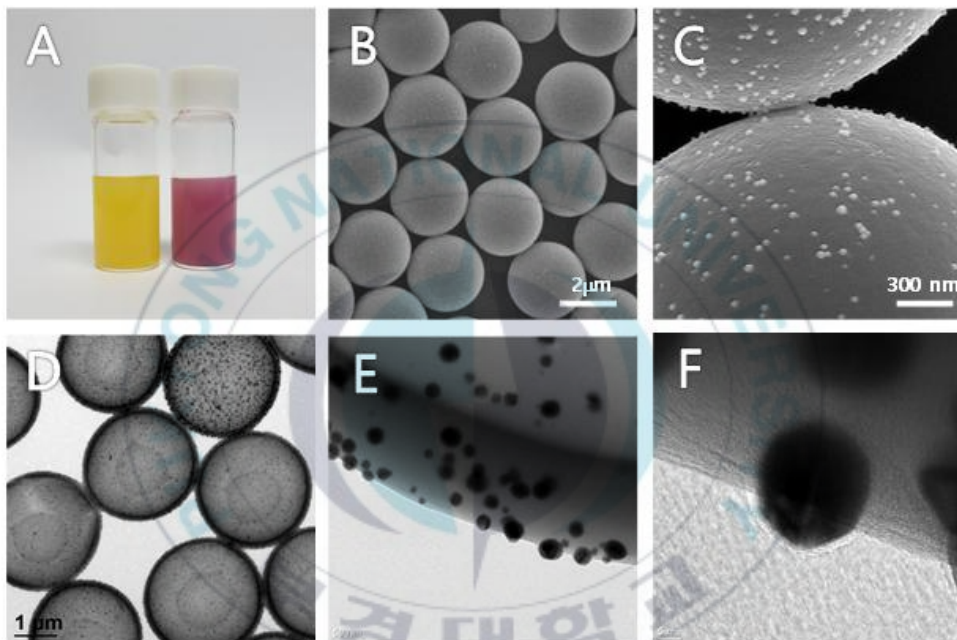


Figure III-5. TEM images of PS microparticles and after being aged in ethanol and water medium containing AgNO_3 and PVP at 70°C for different time periods: (A) 30 min, (B) 1 h, (C) 2 h, and (D) 5 h.

osmolality of the solutions, and thus the final Ag nanocrystals-embedded PS microparticles exhibited the solid structure^[100-101].

The galvanic replacement reaction is a facile approach to generating a variety of bimetallic nanostructures with versatility^[102-104]. The galvanic replacement reaction consists of a redox process between a metal structure (a sacrificial template), and metal ions in solution. The difference in the electrical reduction potential between the sacrificial template and the metal ions in solution provides the driving force for the reaction: oxidation and dissolution of the template together with reduction of metal ions from solution and deposition at the surface of the template^[105]. The galvanic replacement reaction has been employed for generating nanostructures based on gold (Au) from Ag nanocrystals as sacrificial templates^[106].

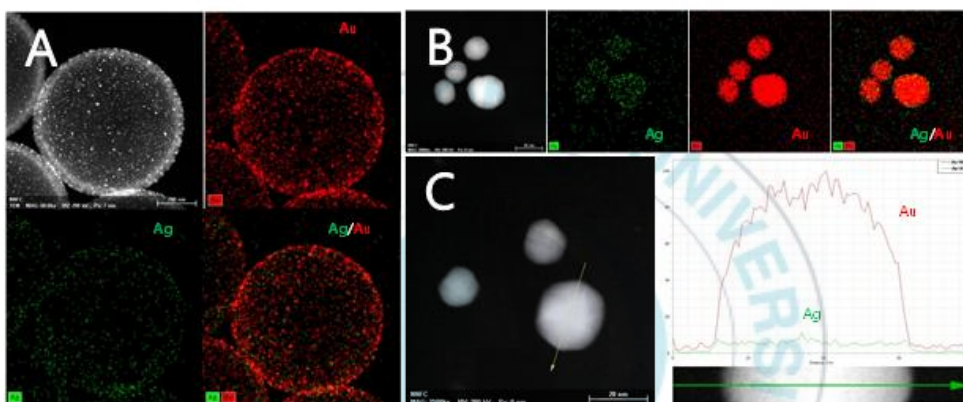
When the formed Ag nanocrystals-embedded PS microparticles were dispersed in ethanol and water medium containing HAuCl_4 and PVP at 70 °C, the yellowish solution became ruby red, which is a characteristic color of gold nanocrystals (see Figure III-6A). Figures III-6B exhibited the SEM images of the resulting PS micr-



Figures III-6. (A) Photograph of Ag nanocrystals-embedded PS microparticles before (left) and after (right) being aged in ethanol and water medium containing HAuCl_4 and PVP at $70\text{ }^\circ\text{C}$ for 24 h. (B-C) SEM images and (D-F) TEM images of the resulting bi-metallic hybrid microparticles.

oparticle, which indicated that the average particles size was increased from 1.84 (± 0.02) μm to 2.71 (± 0.06) μm . An even more magnified SEM image indicated that the microparticles surface was a bit rough and covered by tiny particles (see Figure III-6C). The corresponding TEM images showed that nanoparticles were substantially decorated on the surface of the PS microparticles (see Figure III-6D-III-6F). EDS mapping analysis was conducted to study the relative positions of Au and Ag within the individual PS microparticle. Figure III-7A shows the elemental mapping images for Au and Ag, as well as an overlay of both, within the individual PS microparticles, which demonstrated that the Au/Ag bimetallic nanocrystals were obtained from the galvanic replacement reaction between Ag nanocrystal and AuCl_4^- . Figures III-7B-III-7C displayed the elemental mapping images for individual nanoparticles on the surface of PS microparticles, showing that most appeared homogeneously alloyed but the Au content in the particles was quite higher.

The striking feature observed in the TEM images shown in Figure III-6D-III-6E was the strong contrast between the dark edge and the bright center. The image clearly indicated that the



Figures III-7. EDS elemental mapping images of (A) Au/Ag bi-metallic nanocrystals covered PS microparticles, and (B) Au/Ag bimetallic nanocrystals on PS microparticles. (C) Au and Ag elemental profiles along the green across the of Au/Ag bimetallic nanocrystal on PS microparticles. The scale bars in each image represents (A) 700 nm, and (B-C) 20 nm, respectively.

hybrid microparticles had a hollow structure. Accompanied by the galvanic replacement reactions, the structural transformation occurred during the aging process. As mentioned above, when the Ag nanocrystal-embedded PS microparticles formed, the uptake of continuous phase by the particles was observed at the early stage of the aging process. As the aging time was extended, however, the ethanol and water absorbed in the early stage of aging process migrated to outside the particles because of the osmotic pressure acting from the PS microparticle inside out, which was found to be generated from the Ag^+ ions adsorbed on to the particles' surface. However, when the adsorbed Ag^+ ions were reduced by ethanol and the Ag nanocrystals were formed, the effect of osmotic pressure would disappear. In addition, the precursor for Au nanocrystals (AuCl_4^-) has negative charge and it would not be adsorbed on the PS microparticles surfaces. In such conditions, ethanol and water molecules were continuously absorbed into the PS microparticles. Then, the absorbed water and ethanol molecules were coalesced into bigger domains, resulting in the formation of large cavity as shown Figure III-6D, driven by a tendency to minimize of the surface free energy.

When the PS microparticles saturated with water and ethanol were cooled to room temperature (below glass transition), the domains were immobilized due to the reduced chain mobility of the polymer. After removal of water, hollow PS microparticles with smooth surface and a nearly uniform shell thickness were produced. From these results, it was confirmed that the Ag nanocrystals-embedded solid PS microparticles transformed into hollow Au/Ag bimetallic nanocrystal-covered PS microparticles by the galvanic replacement reaction and the uptake of continuous phase by the particles.

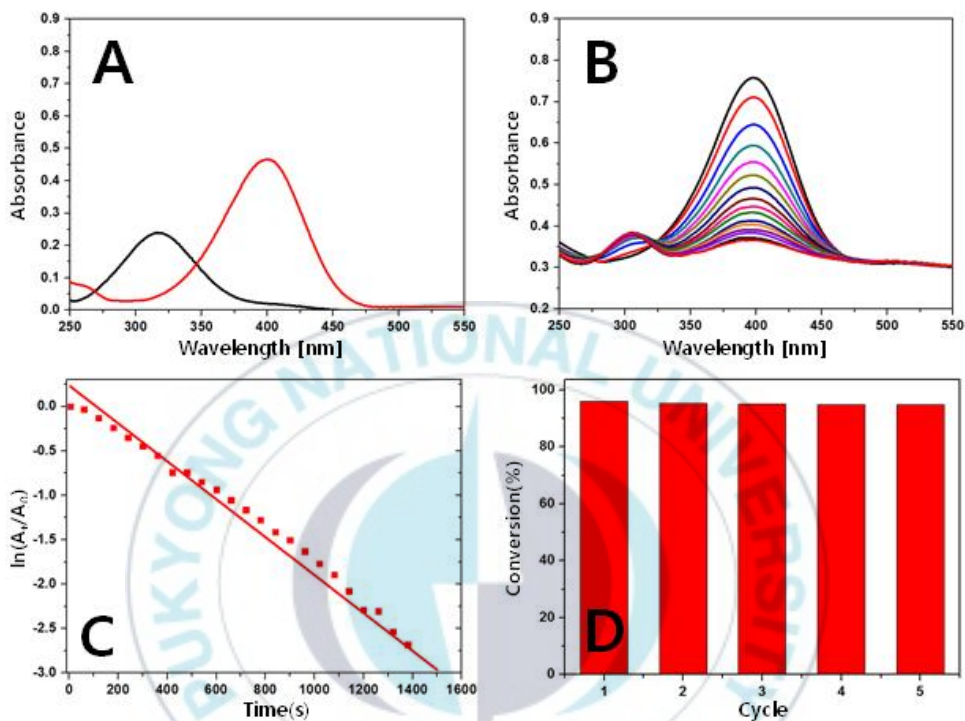
The morphology and compositional results mentioned above motivated us to explore the catalytic activity of the hollow Au/Ag bimetallic nanocrystal and PS hybrid microparticles. The reduction of 4-nitrophenol (4-NP) to 4-aminophenol (4-AP) by NaBH_4 as reducing agent has been widely used to manufacture 4-AP that is commercially important for uses as photographic developers, corrosion inhibitor, anticorrosion-lubricants, and hair-dyeing agents^[70,108]. Various metal nanocrystals including Cu, Ag, Au, Pd, and Pt has been used as the catalyst. However, one fatal drawback for the usage of metal nanocrystals as the catalyst is

that addition of NaBH_4 can destroy their colloidal stability, leading the catastrophic aggregation and deactivation of catalytic performance. This problem can be addressed by depositing the metal nanocrystals on the surface of the polymeric support, which allows the nanocrystals to retain high stability and activity, and enable easy to effective separation from the reaction system for reuse. The hollow Au/Ag bimetallic nanocrystal and PS hybrid microparticles prepared in the present study can be used as excellent catalyst for the reduction of 4-NP to 4-AP because the metal nanocrystals were uniformly deposited on the surface of PS microspheres. In addition, the nanocrystals were bimetallic, composed with Au and Ag, and their size was quite low (less than 20 nm). It has been reported that a lower size of noble metal nanocrystals can led to a higher catalytic activity.

The reduction of 4-NP to 4-AP was carried out in a quart cuvette in the presence of 0.1 mL of as-prepared aqueous hybrid microparticles suspension and 1.4 mL of aqueous 4-NP solution without stirring. Sodium borohydride (NaBH_4) was added after well mixing of the catalysts and 4-NP. The reduction of 4-NP can be easily monitored by UV-vis spectrometer. Monitored by UV-vis

spectrometer, the original 4-NP aqueous solution displays a typical absorption peak at nearly 317 nm as shown in Figure III-8A. The conversion of 4-NP to 4-AP occurs via an intermediate 4-nitrophenolate ion formation. After addition of NaBH_4 into the solution, the color of the solution changed from light yellow to intense yellow. The original peak at 317 was shifted into nearly 400 nm by the addition of due to the formation of 4-nitrophenolate ion (see Figure III-8A). By addition of the hollow Au/Ag bimetallic nanocrystal-covered PS microparticles into the solution, the intense yellow color faded with time because of the formation of 4-nitrophenolate ion in to 4-AP. The corresponding time-dependent UV-vis absorption spectra are shown in Figure III-8B. In the present of the hollow Au-Ag nanocrystals PS hybrid microparticles and NaBH_4 , the intensity of the absorption peak at 400 nm gradually decreased with time and after nearly 7 min it fully disappeared. In the meantime, a new absorption peak appeared at 398 nm and progressively increased in intensity. This new peak is attributed to the typical absorption of 4-aminophenol.

Since the concentration of NaBH_4 greatly exceeds that of 4-NP, the reduction rate can be assumed to be independent of NaBH_4



Figures III-8. (A) UV-vis absorption spectra of 4-NP before and after mixing with NaBH₄. (B) Time-dependent UV-vis absorption spectra and (C) plot of $\ln(A_t/A_0)$ vs time for the catalytic reduction of 4-NP by NaBH₄ in the presence of hollow Au/Ag bimetallic nanocrystals PS hybrid microparticles. (D) Recyclable catalytic ability of the hybrid microparticles for the reduction of 4-NP.

concentration. Therefore, the catalytic rate constant (k) in this case can be evaluated by studying the pseudo-first-order kinetics with respect to 4-NP concentration. Figure III-8C showed that there is a good linear relation between $\ln(A_t/A_0)$ at time t . Here, A_t stands for absorbance at any time t and A_0 for absorbance at time 0. Rate constants (k) can be calculated from the slope of the linear section of the plot, which was measured to be $2.17 \times 10^{-3} \text{ s}^{-1}$. In order to compare the catalytic activity of current catalyst with the previously reported ones, the activity parameters $\kappa = k/m$ (the ratio of rate constant k to the total mass of the catalyst added) was used. In the catalytic activity experiment, 0.4 mg of hollow hybrid microparticles was added. In order to determine the mass for the bimetallic nanocrystals in the hollow microparticles, TGA analysis was conducted out, which showed that the content of bimetallic nanocrystals was nearly 6 wt%. The activity parameters in the present study was found to be 90.42, which is high than the previously reported values. The reusability is another important feature for the supported heterogeneous catalyst. In this work, the hollow hybrid microparticles can be separated out from the reaction system easily by centrifugation owing to

the large size of hollow microparticles. Figure III-8D shows that the high conversion of reduction of 4-NP were obtained in all five reaction time, indicating a high recyclability.

The galvanic replacement reaction has been successfully extended to other noble metals, such as Pt and Pd^[108]. When the Ag nanocrystals-embedded PS microparticles were dispersed in ethanol and water medium containing K₂PtCl₄ and PVP at 70 °C, the yellowish solution became grayish brown. Figure III-9A exhibited the SEM images of the resulting PS microparticle, which indicated that the average particles size was increased from 1.84 (± 0.02) μm to 2.69 (± 0.02) μm during the galvanic replacement reaction process. The corresponding TEM images showed that nanoparticles were substantially decorated on the surface of the PS microparticles (see Figure III-9B). However, the nanocrystal size and shapes were distinctly different from those observed in the Au-Ag system. This is because, unlike Au, Pt does not readily undergo solid-solid diffusion with Ag at temperature below 900 K. By addition of the Pt/Ag bimetallic nanocrystal-covered PS microparticles into the solution, the intense yellow color faded with time because of the formation of 4-nitro-

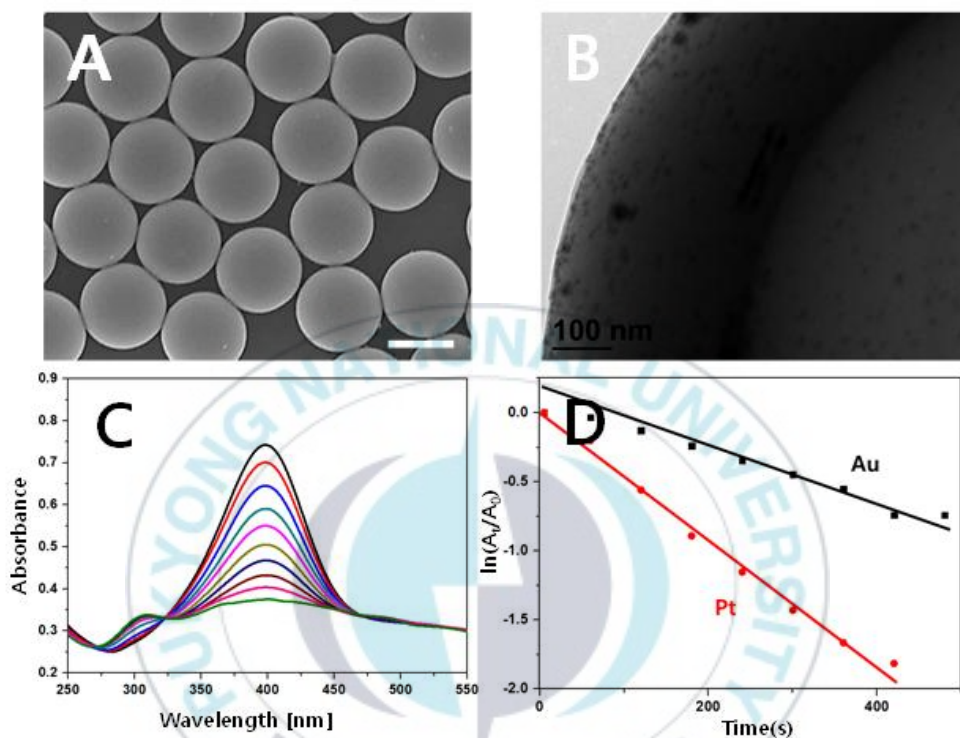
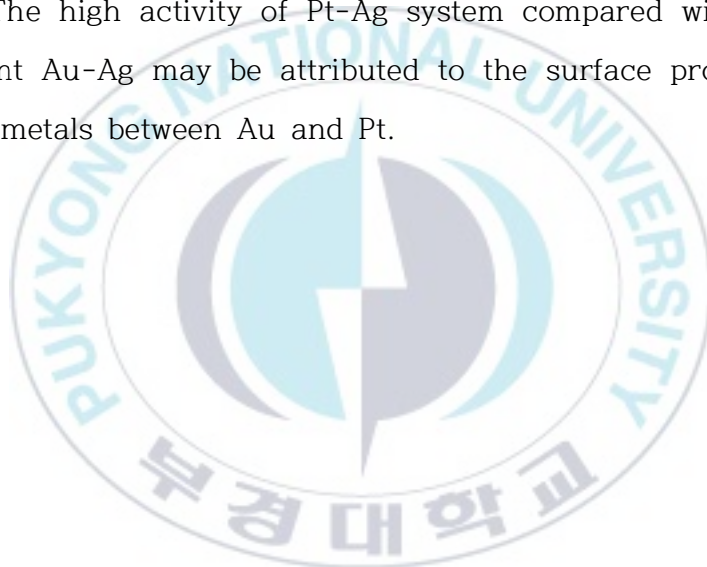


Figure III-9. (A) SEM and (B) TEM images of Ag nanocrystals-embedded PS microparticles and after being aged in ethanol and water medium containing K_2PtCl_4 and PVP at 70 °C for 24 h. (C) Time-dependent UV-vis absorption spectra and (D) plot of $\ln(A_t/A_0)$ vs time for the catalytic reduction of 4-NP by $NaBH_4$ in the presence of hollow Pt/Ag bimetallic nanocrystals PS hybrid microparticles.

phenolate ion in to 4-AP. The corresponding time-dependent UV-vis absorption spectra are shown in Figure III-9C. Rate constants (k) can be calculated from the slope of the linear section of the plot, which was measured to be $4.57 \times 10^{-3} \text{ s}^{-1}$, which was even better than Au-Ag nanocrystal system as shown in Figures III-9D. The high activity of Pt-Ag system compared with that of equivalent Au-Ag may be attributed to the surface properties of the two metals between Au and Pt.



III-4. Conclusions

A facile synthetic method which adopted the heterophase polymer dispersion system was developed for producing hollow bimetallic nanocrystals-polystyrene hybrid microparticles. In the synthesis, solid Ag nanocrystals-embedded PS microparticles were prepared by *in situ* reduction of silver precursor on the PS microparticles and used as seed particles. When the seed particles were dispersed in an ethanol-water mixture containing H_{Au}Cl₄ or K₂PtCl₄ precursors, they transformed into hollow Au/Ag or Pt/Ag nanocrystal-covered PS microparticles by the galvanic replacement reaction and the uptake of continuous phase by the particles. During these overall reactions, a non-toxic reducing agent and environmentally benign solvent media were used. The prepared hollow bimetallic hybrid microparticles showed excellent catalytic activity and reusability at low catalyst concentration during the reduction of 4-NP by NaBH₄, indicating that they will have great potential as reusable heterogeneous catalyst for practical applications.

References

- (1) Edlund, U., & Albertsson, A. C. (2002). Degradable polymer microspheres for controlled drug delivery. In Degradable aliphatic polyesters. Springer Berlin Heidelberg, 67-112.
- (2) Freiberg, S., & Zhu, X. X. (2004). Polymer microspheres for controlled drug release. International journal of pharmaceuticals, 282(1), 1-18.
- (3) Lynn, D. M., Amiji, M. M., & Langer, R. (2001). pH-responsive polymer microspheres: Rapid release of encapsulated material within the range of intracellular pH. Angewandte Chemie International Edition, 40(9), 1707-1710.
- (4) Ma, Y., & Zhang, Q. (2012). Preparation and characterization of monodispersed PS/Ag composite microspheres through modified electroless plating. Applied surface science, 258(19), 7774-7780.
- (5) Abdelrahman, A. I., Thickett, S. C., Liang, Y., Ornatsky, O., Baranov, V., & Winnik, M. A. (2011). Surface functionalization methods to enhance bioconjugation in metal-labeled poly-

- styrene particles. *Macromolecules*, 44(12), 4801-4813.
- (6) Okubo, M. (Ed.). (2005). *Polymer particles*. Springer Science & Business Media.
- (7) Dendukuri, D., Tsoi, K., Hatton, T. A., & Doyle, P. S. (2005). Controlled synthesis of nonspherical microparticles using microfluidics. *Langmuir*, 21(6), 2113-2116.
- (8) Arshady, R. (1992). Suspension, emulsion, and dispersion polymerization: A methodological survey. *Colloid & Polymer Science*, 270(8), 717-732.
- (9) Asua, J. M. (2004). Emulsion polymerization: from fundamental mechanisms to process developments. *Journal of Polymer Science Part A: Polymer Chemistry*, 42(5), 1025-1041.
- (10) Nomura, M., Tobita, H., & Suzuki, K. (2005). Emulsion polymerization: kinetic and mechanistic aspects. In *Polymer particles*. 1-128. Springer Berlin Heidelberg.
- (11) Liu, B., Zhang, M., Liu, Y., Tan, Z., Zhou, C., & Zhang, H. (2015). Particle nucleation and growth in the emulsion polymerization of styrene: effect of monomer/water ratio and electrolyte concentration. *Journal of Macromolecular Science, Part A*, 52(2), 147-154.

- (12) Cho, Y. S., Shin, C. H., & Han, S. (2016). Dispersion Polymerization of Polystyrene Particles Using Alcohol as Reaction Medium. *Nanoscale research letters*, 11(1), 46.
- (13) Rudin, A., & Choi, P. (2012). *The elements of polymer science and engineering*. Academic press.
- (14) Guan, G., Zhang, Z., Wang, Z., Liu, B., Gao, D., & Xie, C. (2007). Single-Hole Hollow Polymer Microspheres toward Specific High-Capacity Uptake of Target Species. *Advanced Materials*, 19(17), 2370-2374.
- (15) Han, J., Liu, Y., & Guo, R. (2009). Reactive template method to synthesize gold nanoparticles with controllable size and morphology supported on shells of polymer hollow microspheres and their application for aerobic alcohol oxidation in water. *Advanced Functional Materials*, 19(7), 1112-1117.
- (16) Li, G., Yang, X., Wang, B., Wang, J., & Yang, X. (2008). Monodisperse temperature-responsive hollow polymer microspheres: synthesis, characterization and biological application. *Polymer*, 49(16), 3436-3443.
- (17) Ramli, R. A. (2017). Hollow polymer particles: a review. *RSC Advances*, 7(83), 52632-52650.

- (18) Donath, E., Sukhorukov, G. B., Caruso, F., Davis, S. A., & Möhwald, H. (1998). Novel hollow polymer shells by colloid-templated assembly of polyelectrolytes. *Angewandte Chemie International Edition*, 37(16), 2201-2205.
- (19) Konishi, Y., Okubo, M., & Minami, H. (2003). Phase separation in the formation of hollow particles by suspension polymerization for divinylbenzene/toluene droplets dissolving polystyrene. *Colloid and Polymer Science*, 281(2), 123-129.
- (20) Discher, B. M., Won, Y. Y., Ege, D. S., Lee, J. C., Bates, F. S., Discher, D. E., & Hammer, D. A. (1999). Polymersomes: tough vesicles made from diblock copolymers. *Science*, 284(5417), 1143-1146.
- (21) Koo, H. Y., Chang, S. T., Choi, W. S., Park, J. H., Kim, D. Y., & Velev, O. D. (2006). Emulsion-based synthesis of reversibly swellable, magnetic nanoparticle-embedded polymer microcapsules. *Chemistry of materials*, 18(14), 3308-3313.
- (22) Im, S. H., Jeong, U., Xia, Y (2005). Polymer Hollow Particles with Controllable Holes in the Their Surfaces. *Nat. Mater.* 4, 671-675.
- (23) Lou, X. W., Archer, L., Yang, Z (2008). Hollow

- Micro-/Nanostructures: Synthesis and Applications. *Adv. Mater.* 20, 3987–4019.
- (24) Caruso, F (2000). Hollow Capsule Processing through Colloidal Templating and Self-Assembly. *Chem. - Eur. J.* 6, 413–419.
- (25) Lv, H., Zhang, K., Yu, K., Yao, T., Zhang, X., Zhang, J., Yang, B (2008). Facile Fabrication of Monodisperse Polymer Hollow Spheres. *Langmuir*, 24, 13736–13741.
- (26) Meier, W (2000). Polymer Nanocapsules. *Chem. Soc. Rev.* 29, 295–303.
- (27) Lvov, Y., Antipov, A. A., Mamedov, A., Mohwald, H., Sukhorukov, G. B (2001). Urease Encapsulation in Nanoorganized Microshells. *Nano Lett.* 1, 125–128.
- (28) Xu, X., Asher, S. A (2004). Synthesis and Utilization of Monodisperse Hollow Polymeric Particles in Photonic Crystals. *J. Am. Chem. Soc.* 126, 7940–7945.
- (29) Kida, T., Mouri, M., Akashi, M (2006). Fabrication of Hollow Capsules Composed of Poly(methyl methacrylate) Stereocomplex Films. *Angew. Chem., Int. Ed.* 45, 7534–7536.
- (30) Han, J., Song, G., Guo, R (2007). Synthesis of Polymer Hollow

- Spheres with Holes in Their Surfaces. *Chem. Mater.* 19, 973–975.
- (31) Minami, H., Kobayashi, H., Okubo, M (2005). Preparation of Hollow Polymer Particles with a Single Hole in the Shell by SaPSeP. *Langmuir*, 21, 5655–5658.
- (32) Wang, L., Liang, H., Wang, F., Huang, L., Liu, Z., Dong, Z (2013). One-Step Synthesis of Uniform Double-Shelled Polystyrene/Poly(otoluidine) Composite Hollow Spheres. *Langmuir*, 29, 5863–5868.
- (33) Weng, H., Huang, X., Wang, M., Ji, X., Ge, X (2013). Formation of Cagelike Sulfonated Polystyrene Microspheres via Swelling-Osmosis Process and Loading of CdS Nanoparticles. *Langmuir*, 29, 15367–15374.
- (34) Jose, J., Kamp, M., van Blaaderen, A., Imhof, A (2014). Unloading and Reloading Colloidal Microcapsules with Apolar Solutions by Controlled and Reversible Buckling. *Langmuir*, 30, 2385–2393.
- (35) Jeong, U., Im, S. H., Camargo, P. H. C., Kim, J. H., Xia, Y (2007). Microscale Fish Bowls: A New Class of Latex Particles with Hollow Interiors and Engineered Porous Structures in

- Their Surfaces. *Langmuir*, 23, 10968–10975.
- (36) Chen, D., Jiang, M (2005). Strategies for Constructing Polymeric Micelles and Hollow Spheres in Solution via Specific Intermolecular Interactions. *Acc. Chem. Res.* 38, 494–502.
- (37) Tian, Q., Yu, D., Zhu, K., Hu, G., Zhang, L., Liu, Y (2016). Multihollow Polymer Microspheres with Enclosed Surfaces and Compartmentalized Voids Prepared by Seeded Swelling Polymerization Method. *J. Colloid Interface Sci.* 473, 44–51.
- (38) Meng, X., Guan, Y., Niu, Z., Qiu, D (2013). Facile Preparation Route toward Speckled Colloids via Seeded Polymerization. *Langmuir*, 29, 2152–2158.
- (39) Wang, G., Dou, H., Sun, K (2012). Facile Synthesis of Hollow Polymeric Microparticles Possessing Various Morphologies via Seeded Polymerization. *Colloid Polym. Sci.* 290, 1867–1877.
- (40) Dendukuri, D., Doyle, P. S (2009). The Synthesis and Assembly of Polymeric Microparticles Using Microfluidics. *Adv. Mater.* 21, 4071–4086.
- (41) Wang, W., Ren, G., Yang, Y., Cai, W., Chen, T (2015). Synthesis and Properties Study of the Uniform Nonspherical

- Styrene/Methacrylic Acid Copolymer Latex Particles. *Langmuir*, 31, 105–109.
- (42) Sacanna, S., Korpics, M., Rodriguez, K., Colon-Melendez, L., Kim, S. H., Pine, D. J., Yi, G. R (2013). Shaping Colloids for Self-Assembly. *Nat. Commun.* 4, 1688.
- (43) Kim, S. H., Hollingsworth, A. D., Sacanna, S., Chang, S. J., Lee, G., Pine, D. J., Yi, G. R (2012). Synthesis and Assembly of Colloidal Particles with Sticky Dimples. *J. Am. Chem. Soc.* 134, 16115–16118.
- (44) Chen, J., Clay, N. E., Park, N. H., Kong, H (2015). Non-Spherical particles for Targeted Drug Delivery. *Chem. Eng. Sci.* 125, 20–24.
- (45) Paine, J., Luymes, W., McNulty, J (1990). Dispersion Polymerization of Styrene in Polar Solvents. 6. Influence of Reaction Parameters on Particle Size and Molecular Weight in Poly(N-vinylpyrrolidone)-Stabilized Reactions. *Macromolecules* 23, 3104–3109.
- (46) Tseng, M., Lu, Y. Y., El-Aasser, M. S., Vanderhoff, J. W (1986). Uniform Polymer Particles by Dispersion polymerization in Alcohol. *J. Polym. Sci., Part A: Polym. Chem.* 24,

- 2995–3007.
- (47) Kawaguchi, S., Ito, K. Dispersion Polymerization (2005). Adv. Polym. Sci. 175, 299–328.
- (48) Cox, R. A., Creasey, J. M., Wilkinson, M. C (1974). Anomalies in Particle Shape during Seeded Growth of Polystyrene Latices. Nature, 252, 468–469.
- (49) Goodall, A. R., Wilkinson, M. C., Hearn, J (1977). Mechanism of Emulsion Polymerization of Styrene in Soap-Free Systems. J. Polym. Sci., Polym. Chem. Ed. 15, 2193–2218.
- (50) Goodall, A. R., Wilkinson, M. C., Hearn, J (1975). Formation of Anomalous Particles during the Emulsifier-Free Polymerization of Styrene. J. Colloid Interface Sci. 53, 327–331.
- (51) Tauer, K (1998). Comment on the Development of Particle Surface Charge Density during Surfactant-Free Emulsion Polymerization with Ionic Initiators. Macromolecules 31, 9390–9391.
- (52) Tauer, K., Riedelsberger, K., Deckwer, R., Zimmermann, A., Dautzenberg, H., Thieme, J (2000). A New Way to Control Particle Morphology in Heterophase Polymerizations.

- Macromol. Symp. 155, 95–104.
- (53) Tauer, K., Deckwer, R., Kuhn, I., Schellenberg, C (1999). A Comprehensive Experimental Study of Surfactant-free Emulsion Polymerization of Styrene. *Colloid Polym. Sci.* 277, 607–626.
- (54) Zhu, M. Q., Chen, G. C., Li, Y. M., Fan, J. B., Zhu, M. F., Tang, Z (2011). One-Step Template-Free Synthesis of Monoporous Polymer Microspheres with Uniform Sizes via Microwave-Mediated Dispersion polymerization. *Nanoscale*, 3, 4608–4612.
- (55) Liu, D., Peng, X., Wu, B., Zheng, W., Chuong, T. T., Li, J., Sun, S., Stucky, G. D (2015). Uniform Concave Polystyrene-Carbon Core-Shell Nanospheres by a Swelling Induced Buckling Process. *J. Am. Chem. Soc.* 137, 9772–9775.
- (56) Lee, J., Ha, J. U., Choe, S., Lee, C. S., Shim, S. E (2006). Synthesis of Highly Monodisperse Polystyrene Microspheres via Dispersion Polymerization Using an Amphoteric Initiator. *J. Colloid Interface Sci.* 298, 663–671.
- (57) Ha, S. T., Park, O. O., Im, S. H (2010). Size Control of Highly

- Monodisperse Polystyrene Particles by Modified Dispersion Polymerization. *Macromol. Res.* 18, 935–943.
- (58) Choi, H. K., Kim, M. H., Im, S. H., Park, O. O (2009). Fabrication of Ordered Nanostructured Arrays Using Poly(dimethylsiloxane) Replica Molds Based on Three-Dimensional Colloidal Crystals. *Adv. Funct. Mater.* 19, 1594–1600.
- (59) Burda, C., Che, X., Narayanan, R., El-Sayed, M. A (2005). Chemistry and Properties of Nanocrystals of Different Shapes. *Chem. Rev.* 105, 1025-1102.
- (60) Xia, Y., Xiong, Y., Lim, B., Skrabalak, S. E (2008). Shape-Controlled Synthesis of Metal Nanocrystals: Simple Chemistry Meets Complex Physics. *Angew. Chem. Int.* 48, 60-103.
- (61) Rycenga, M., Cobley, C. M., Zeng, J., Li, W., Moran C. H., Zhang, Q., Qin, D., Xia, Y (2011). Controlling the Synthesis and Assembly of Silver Nanostructures for Plasmonic Applications. *Chem. Rev.* 111, 3669-3712.
- (62) Zhang, Li., Liu, W., Xu, G (2012). Synthesis and Applications of Noble Metal Nanocrystals with High-Energy Facets. *Nanotoday.* 7, 586-605.

- (63) Wu, Y., Wang, D., Li, Y (2014). Nanocrystals from Solutions: Catalysts. *Chem. Soc. Rev.* 43, 2112-2124.
- (64) Quan, Z., Wang, Y., Fang, J (2013). High-Index Faceted Noble Metal Nanocrystals. *Acc. Chem. Res.* 46, 191-202.
- (65) Xie, S., Choi, S. I., Xia, X., Xia, Y (2013). Catalysis on Faceted Noble-Metal nanocrystals: Both Shape and Size. *Matter. Curr. Opin. Chem. Eng.* 2, 142.
- (66) Zhang, H., Jin, M., Xia, Y (2012). Noble-Metal Nanocrystals with Concave Surfaces: Synthesis and Applications. *Angew. Chem. Int. Ed.* 51, 7656-7673.
- (67) Liu, H., Nosheen, F., Wang, Xun (2015). Noble Metal Alloy complex Nanostructures: Controllable Synthesis and Their Electrochemical Properties. *Chem. Soc. Rev.* 44, 3056-3078.
- (68) Fan, Z., Zhang, H (2016). Template Synthesis of Noble Metal Nanocrystals with Unusual Crystal Structures and Their Catalytic Applications. *Acc. Chem. Res.* 49, 2841-2850.
- (69) Zhang, P., Shao, C., Zhang, Z., Zhang, M., Mu, J., Guo, Z., Liu, Y (2011). In Situ Assembly of Well-Dispersed Ag Nanoparticles (AgNPs) on Electrospun Carbon Nanofibers (CNFs) for Catalytic Reduction of 4-Nitrophenol. *Nanoscale.*

- 3, 3357-3363.
- (70) Geng, Q., Du, J (2014). Reduction of 4-Nitrophenol Catalyzed by Silver Nanoparticles Supported Polymer Micelles and Vesicles. *RSC Adv.* 4, 16425-16428.
- (71) Han, J., Liu, Y., Guo, R (2008). Reactive Template Method to Synthesize Gold Nanoparticles with Controllable Size and Morphology Supported on Shells of Polymer Hollow Microspheres and Their Applications for Aerobic Alcohol Oxidation in Water. *Adv. Funct. Mater.* 19, 1112-1117.
- (72) Li, Y., Wu, Y., Gao, Y., Sha, S., Hao, J., Cao, G., Yang, C (2013). A Facile Method to Fabricate Polystyrene/Silver Composite Particles and Their Catalytic Properties. *RSC Adv.* 3, 26361.
- (73) Sebastian, V., Lee, S. K., Jensen, K. F (2014). Engineering the Synthesis of Silica-Gold Nano-Urchin Particles Using Continuous Synthesis. *Nanoscale.* 6, 13228-13235.
- (74) Du, J., O'Reilly R. K (2009). Advances and Challenges in Smart and Functional Polymer Vesicles. *Soft Matter.* 5, 3544-3561.
- (75) Zhao, P., Reng, X., Huang, D., Yang, G., Astruc, D (2015).

- Basic Concepts and Recent Advances in Nitrophenol Reduction by Gold- and Other Transition Metal Nanoparticles. *Coord. Chem. Rev.* 287, 114-136.
- (76) Hu, W., Liu, B., Wang, Q., Liu, Y., Jing, P., Yu, S., Liu, L., Zhang, J (2013). A Magnetic Double-Shell Microsphere as a Highly Efficient Reusable Catalyst for Catalytic Applications. *Chem. Comm.* 49, 7596-7598.
- (77) Wang, X., Long, Y., Wang, Q., Zhang, H., Huang, X., Zhu, R., Teng, P., Liang, L., Zheng, H (2013). Reduced State Carbon Dots as Both Reductant and Stabilizer for the Synthesis of Gold Nanoparticles. *Carbon.* 64, 499-506.
- (78) Lim, M. H., Ast, D. G (2011). Free-Standing Thin Films Containing Hexagonally Organized Silver Nanocrystals in a Polymer Matrix. *Adv. Mater.* 13, 718-721.
- (79) Trojanowska, A., Pazos-Perez, N., Panisello, C., Gumi, T., Guerrini, L., Alvarez-Puebla, R. A (2015). Plasmonic-Polymer Hybrid Hollow Microbeads for Surface-Enhanced Raman Scattering (SERS) Ultradetection. *J. Colloid Interf. Sci.* 460, 128-134.
- (80) Park, K. H., Kim, M. H., Im, S. H., Park, O. O (2016).

- Electrically Bistable Ag Nanocrystal-Embedded Metal-Organic Framework Microneedles. *RSC Adv.* 6, 64885-64889.
- (81) P. Falcaro, R. Ricco, A. Yazdi, I. Imaz, S. Furukawa, D. Maspoch, R. Ameloot, J. D. Evans, C. J. Doonan (2016). Application of Metal and Metal Oxide Nanoparticle@MOFs. *Coord. Chem. Rev.* 307, 237-254.
- (82) Jiang, H. L., Akita, T., Ishida, T., Haruta, M., Xu, Q (2011). Synergetic Catalyst of Au@Ag Core-Shell Nanoparticles Stabilized on Metal-Organic Framework. *J. Am. Chem. Soc.* 133, 1304-1306.
- (83) Xia, B., He, F., Li, L (2013). Preparation of Bimetallic Nanoparticles Using a Facile Green Synthesis Method and Their Application. *Langmuir.* 29, 4901-4907.
- (84) Huang, J., Vongehr, S., Tang, S., Lu, H., Meng, X (2010). Highly Catalytic Pd-Ag Bimetallic Dendrites. *J. Phys. Chem. C.* 114, 15005-15010.
- (85) Huang, J., Vongehr, S., Tang, S., Lu, H., Shen, J., Meng, X (2013). Ag Dendrite-Based Au/Ag Bimetallic Nanostructures with Strongly Enhanced Catalytic Activity. *Langmuir.* 29, 4901-4907.

- (86) Park, S. H., Kim, J., Lee, W. E., Byun, D. J., Kim, M. H (2017). One-Step Synthesis of Hollow Dimpled Polystyrene Microparticles by Dispersion Polymerization. *Langmuir*. 33, 2275-2282.
- (87) Paine, J., Luymes, W., McNulty, J (1990). Dispersion Polymerization of Styrene in Polar Solvents. 6. Influence of Reaction Parameters on Particle Size and Molecular Weight in Poly(N-vinylpyrrolidone)-Stabilized Reactions. *Macromolecules*. 23, 3104-3109.
- (88) Tseng, M., Lu, Y. Y., El-Aasser, M. S., Vanderhoff, J. W (1986). Uniform Polymer Particles by Dispersion polymerization in Alcohol. *J. Polym. Sci. Part A: Polym. Chem.* 24, 2995.-3007
- (89) Kawaguchi, S., Ito, K (2005). Dispersion Polymerization. *Adv. Polym. Sci.* 175, 299-328.
- (90) Na, K., Choi, K. M., Yaghi, O. M., Somorjai, G. A (2014). Metal Nanocrystals Embedded in Single Nanocrystals of MOFs Give Unusual Selectivity as Heterogeneous Catalysts. *Nano Lett.* 14, 5979-5983.
- (91) Bardhan, R., Ruminski, A. M., Brand, A., Urban, J. J (2011).

- Magnesium Nanocrystal-Polymer Composites: A New Platform for Designer Hydrogen Storage Materials. *Energy Environ. Sci.* 4, 4882-4895.
- (92) Jo, C., Pugal, D., Oh, I. K., Kim, K. J., Asaka, K (2013). Recent Advances in Ionic Polymer-Metal Composite Actuators and Their Modelling and Applications. *Prog. Polym. Sci.* 38, 1037-1066.
- (93) Kim M. H., Kwak, S. K., Im, S. H., Lee, J. B., Choi, K. Y., Byun, D. J (2014). Maneuvering the Growth of Silver Nanoplates: Use of Halide Ions to Promote Vertical Growth. *J. Mater. Chem. C.* 2, 6165-6170.
- (94) Tian, Q., Yu, D., Zhu, K., Hu, G., Zhang, L., Liu, Y (2016). Multi-Hollow Polymer Microspheres with Enclosed Surfaces and Compartmentalized Voids Prepared by Seeded Swelling Polymerization Method. *J. Colloid. Interface Sci.* 473, 44-51.
- (95) Tsavalas, J. G., Sundberg, D. C (2010). Hydroplasticization of Polymers: Model Predictions and Application to Emulsion Polymers. *Langmuir.* 26, 6960-6966.
- (96) Okubo, M., Kobayashi, H., Huang, C., Miyanga, E., Suzuki, T (2017). Water Absorption Behavior of Polystyrene Particles

- Prepared by Emulsion Polymerization with Nonionic Emulsifiers and Innovative Easy Synthesis of Hollow Particles. *Langmuir*. 33, 3468-3475.
- (97) Kumbhar, A. S., Chumanov, G (2009). Encapsulation of Silver Nanoparticles into Polystyrene Microspheres. *Chem. Mater.* 21, 2835-2839.
- (98) He, J., Perez, M. T., Zhang, P., Liu, Y., Babu, T., Gong, J., Nie, Z (2012). A General Approach to Synthesize Asymmetric Hybrid Nanoparticles by Interfacial Reactions. *J. Am. Chem. Soc.* 134, 3639-3642.
- (99) Kanaharan, M., Shimomura, M., Yabu, H (2014). Fabrication of Gold Nanoparticle-Polymer Composite Particles with Raspberry, Core-Shell and Amorphous Morphologies at Room Temperature via Electrostatic Interactions and Diffusion. *Soft Matter*. 10, 275-280.
- (100) Zhao, Q., Chen, N., Zhao, D., Lu, X (2013). Thermoresponsive Magnetic Nanoparticles for Seawater Desalination. *ACS Appl. Mater. Interfaces*. 5, 11453-11461.
- (101) Guo, C. X., Zhao, D., Zhao, Q., Wang, P., Lu, X (2014). Na⁺-Functionalized Carbon Quantum Dots: A New Draw

- Solute in Forward Osmosis for Sea water Desalination. Chem. Commun. 50, 7318-7321.
- (102) Oh, M. H., Yu T., Yu. S. H., Lim, B., Ko. K. T., Willinger, M. G., Seo, D. H. Kim, B. H., Cho, M. G., Park, J. H., Kang, K., Sung. Y. E., Pinna, N., Hyeon, T (2013). Galvanic Replacement Reactions in Metal Oxide Nanocrystals. Science. 340, 964-968.
- (103) Ruditskiy, A., Xia, Y (2017). The Science and Art of Carving Metal Nanocrystals. ACS Nano. 11, 23-27.
- (104) Xia, X., Wang, Y., Ruditskiy, A., Xia, Y (2013). Galvanic Replacement: A Simple and Versatile Route to Hollow Nanostructures with Tunable and Well-Controlled Properties. Adv. Mater. 25, 6313-6333.
- (105) da Silva, A. G. M., Rodrigues, T. S., Haigh, S. J., Camargo, P. H. C (2017). Galvanic Replacement Reaction: Recent Developments for Engineering Metal Nanostructures Towards Catalytic Applications. Chem. Comm. 53, 7135-7148.
- (106) Kim, M. H., Lu, X., Wiley, B., Lee, E. P., Xia, Y (2008). Morphological Evolution of Single-Crystal Ag Nanospheres during the Galvanic Replacement Reaction with HAuCl_4 . J.

Phys. Chem. C. 112, 7872-7876.

- (107) Rode, C. V., Vaidya, M. J., Chaudari, R. V (1999). Synthesis of p-Aminophenol by Catalytic Hydrogenation of Nitrobenzene. Org. Proc. Res. Dev. 3, 465-470.
- (108) Chen, Jingyi., Wiley, B., McLellan, J., Xiong, Y., Li, Z. Y., Xia, Y (2005). Optical Properties of Pd-Ag and Pt-Ag Nanoboxes Synthesized via Galvanic Replacement Reactions. Nano Lett. 5, 2058-2062.

